New Selenium Catalyzed Reactions and Computational Chemistry to Understand Regio- and Diastereoselectivities: Directed C-H Allylic Amination

Janna L. Berman

A dissertation

submitted in partial fulfillment of the

requirements for the degree of

Doctor of Philosophy

University of Washington

2022

Reading Committee:

Forrest E. Michael, Chair

Robert E. Synovec

Matthew R. Golder

Program Authorized to Offer Degree:

Department of Chemistry

University of Washington

Abstract

New Selenium Catalyzed Reactions and Computational Chemistry to Understand Regio- and Diastereoselectivities: Directed C-H Allylic Amination

Janna L. Berman

Chair of Supervisory Committee:

Associate Professor Forrest E. Michael

Department of Chemistry

Allylic amines are an important class of nitrogen-containing compounds for use in synthesis or medicinal properties. Direct strategies to make allylic amines involve activation of an allylic C-H bond (allylic C-H amination), but often require expensive transition metals. Our group previously developed an alternative method using organoselenium catalysis on aliphatic alkenes.

Herein, we discuss the adaptation of our allylic C-H amination reaction on internal vinylsilanes. The substrate scope features a range of silanes and can incorporate two types of nitrogen nucleophiles, including 4-nitrobenzenesulfonamide ($NsNH_2$) and trifluoroethanol sulfonamide ($TfesNH_2$). We discuss a trend in regioselectivity concerning amination with $NsNH_2$,

where activation of the distal allylic C-H bond is preferred. Unexpectedly, the use of $TfesNH_2$ leads to reduced regioselectivity. Terminal vinylsilanes containing activated allylic positions (benzylic, tertiary) are aminated using the same reaction conditions. The utility of the aminated products is shown in two derivatization reactions, including iododesilylation and directed epoxidation. Our amination reaction is demonstrated on a gram scale and is reproducible.

Computational chemistry is employed to determine a model that describes regioselectivity in amination of vinylsilanes. The DFT reaction coordinate involving distal or proximal allylic C-H amination are featured using a selenium diimide derived from methanesulfonamide, our model of $NsNH_2$. The distal path exhibits an ene barrier that is 1.2 kcal/mol lower in energy than the proximal path. The ene step has asynchronous character, where positive charge build-up at the internal alkenyl carbon is consequential for regioselectivity. We determine the DFT reaction coordinate involving a selenium diimide derived from methyl sulfamate, a model of $TfesNH_2$. A substantially lower ene barrier is observed (~ 4 kcal/mol) and can justify a loss of regioselectivity.

We extend our computational study to focus on diastereoselective outcomes in allylic C-H amination. We investigate how protected alcohols at the homoallylic position of alkenes favor formation of *anti*-1,2-products. Homoallyl fluorides are used as model substrates, and we evaluate three conformations of the C-F bond (anti, inside, or outside). The magnitude of electron donation into the π system is correlated with the energy of the [2,3]-sigmatropic rearrangement transition state. The inside alkoxy effect is attributed to the diastereoselectivity, the first time it is implicated in a [2,3]-sigmatropic rearrangement. The rearrangement transition states for a homoallyl acetate substrate are analyzed and formation of the *anti*-diastereomer is favored by 2.6 kcal/mol.

Further studies include the diastereoselective formation of 1,4-products from *Z*-alkenes containing allylic protected alcohols. We evaluated how conformation of the allylic acetyl group

affected the ene transition state energy. We determined the ene transition states leading to the *syn* or *anti* products, focusing on how the eclipsing atom group affected the barrier. In the transition states with minimized $A_{1,3}$ strain, formation of the *syn*-diastereomer was favored by 0.4 kcal/mol. Diastereoselectivity is rationalized by the preference of the diimide to approach the less sterically hindered side of the alkene.

We next investigated how functional groups (X) could act as directing groups for regioselective allylic C-H amination. The ene transition states are determined with electronically diverse X groups near or remote to the allylic site. Enhanced carbocation character is observed in the ene transition states of 1,1- and 1.2-disubstituted alkenes when X is electron-releasing. Statistical analysis is presented with multivariable linear regressions to predict $\Delta G^{\ddagger}$ and $\Delta\Delta G^{\ddagger}$ in these cases. We also calculate the ene transition states for a range of alkenes containing X groups at the vinylic position. Short Se-C distances and a low ene barrier are generally observed when X is electron releasing. A multivariable linear regression model is presented to predict $\Delta G^{\ddagger}$ in these reactions. Following is a study of the ene transition states for two terpenes (methyl jasmonate and δ-damascone) to propose models that rationalize the regioselective amination.

TABLE OF CONTENTS

LIST OF FIGURES

LIST OF TABLES

LIST OF ABBREVIATIONS

Å:	Angstrom
e:	Electron
rt:	Room Temperature
Ac:	Acetyl
Piv:	Pivaloyl
TBDPS:	*tert*-Butyldiphenylsilyl
$SiMe_2Ph$:	Dimethylphenylsilyl
$SiMe_2Bn$:	Dimethylbenzylsilyl
TES or $SiEt_3$:	Triethylsilyl
TMS or $SiMe_3$:	Trimethylsilyl
Bn:	Benzyl
Me:	Methyl
Et:	Ethyl
Ph:	Phenyl
Cy:	Cyclohexyl
t-Bu:	*tert*-Butyl
NFSI:	*N*-Fluorobenzenesulfonamide
Ms:	Mesyl
Ns:	4-nitrobenzenesulfonyl
Tfes:	2,2,2-Trifluoroethoxysulfonyl
BHT:	Butylated Hydroxytoluene

PG:	Protecting Group
L:	Ligand
p:	para
q:	charge
NBO:	Natural Bond Orbital
DFT:	Density Functional Theory
PCM:	Polarization Continuum Model
Δ:	Delta
$\sigma^{(*)}$:	Sigma bonding (anti-bonding)
$\pi^{(*)}$:	Pi bonding (anti-bonding)
G:	Gibbs Free Energy
H:	Enthalpy Energy
ΔG_{rxn}:	Exothermicity
dr:	Diastereomer Ratio
rr:	Regioisomer Ratio
θ:	Dihedral Angle
Hz:	Hertz
MHz:	Megahertz
mp:	Melting Point
NMR:	Nuclear Magnetic Resonance
ppm:	Parts Per Million
IR:	Infared
hr:	hour

ESI-MS	Electrospray Ionization Mass Spectrometry
kcal:	kilocalorie

Abbreviations for NMR Splitting:

s:	singlet
d:	doublet
t:	triplet
q:	quartet
quin:	quintet
m:	multiplet
br:	broad

ACKNOWLEDGEMENTS

I would like to thank my family (Mom, Dad, Jesimin, Jeremy, Gaby, Kira, & Daria) for their support and encouragement as I pursued my graduate studies. Thank you to my Research advisor Dr. Forrest Michael and my committee members (Robert Synovec, Dr. Matthew Golder, Dr. Ronald Stenkamp, and Dr. Gojko Lalic) for their wonderful guidance and feedback on my thesis. Thank you to my previous research advisors (Dr. Luc Boisvert, Dr. Mike Heinekey, Dr. Nathan Schley) for their mentorship.

DEDICATION

To my parents, Marvin and Victoria Berman

My sisters, Jesimin and Gaby and Kira and Daria,

My brother, Jeremy,

For all your support, love, and encouragement.

Chapter 1. DIRECTED ALLYLIC C-H AMINATION OF VINYLSILANES

Section 1: INTRODUCTION

Nitrogen containing molecules are among a privileged class of compounds that are known to be important for bioactivity and they have led to high specificity with biological targets.[1] This favorable accolade can be attributed to two properties of nitrogen, the basic character of the nitrogen lone pair and the ability of the amino group to act as a hydrogen bond donor or acceptor. Substitution at nitrogen provides further opportunities to enhance drug activity, where this feature has modulated drug action within the human body. For example, normorphine has a nitrogen atom that after methylation, produces the much more potent narcotic called morphine (Figure 1.1).[2]

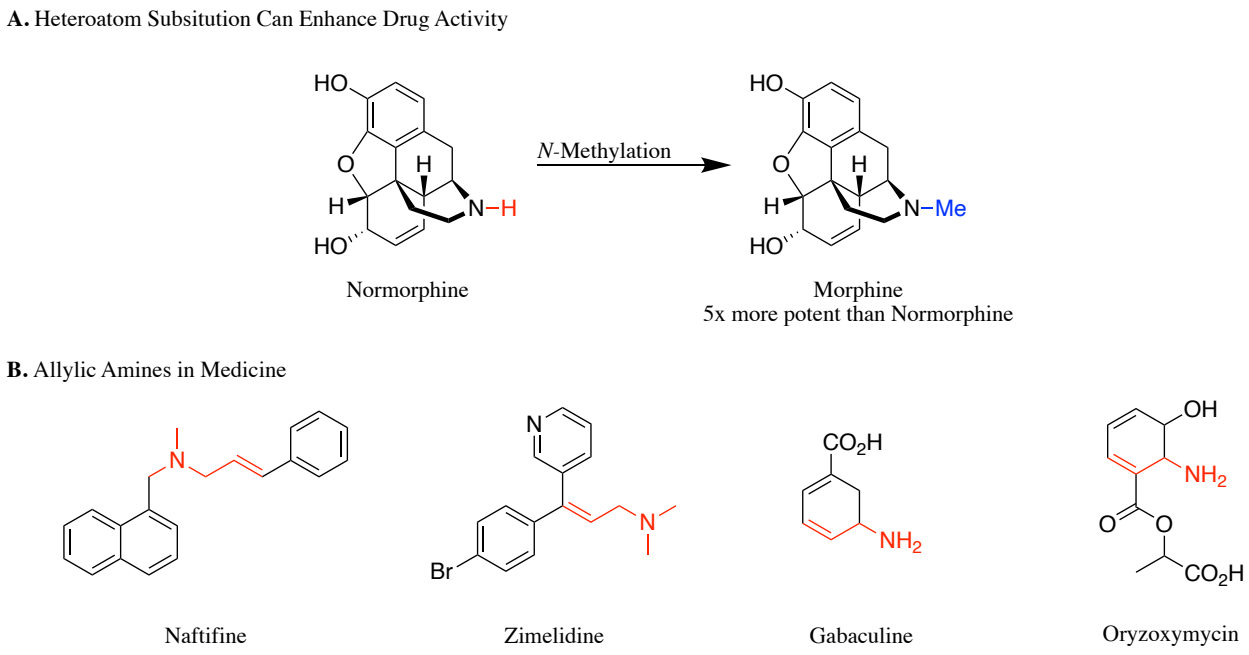

Figure 1.1. Importance of Heteroatom Substitution and Allylic Amine Medicines

This example helps foreshadow a new relevant strategy used in small-molecule discovery programs, and one which nitrogen atoms can be especially beneficial. Whereby a balance of

heteroatom substitution is crucial to a compound's biological activity and potential as a drug.[2] Thus, there remains a demand to design new synthetic strategies that access a range of nitrogen-containing molecules with variable substitution at nitrogen itself.

Allylic amines are a class of nitrogen containing compounds that have garnered attention because they contain dual functionality with a nucleophilic amino group and an olefin. The ability to install different amines at the allylic position would enable faster creation of a library of nitrogen containing molecules and possibly more bioactive compounds. This hypothesis is supported by known examples where allylic amines are present in medicinal molecules, including the antibiotic Oryzoxymycin and the antifungal drug Naftifine (Figure 1.1, part B). Arguably, allylic amines may play a more vital role as synthons towards complex molecules, such as in making amino acids, alkaloids, and carbohydrate derivatives (Figure 1.2).[3]

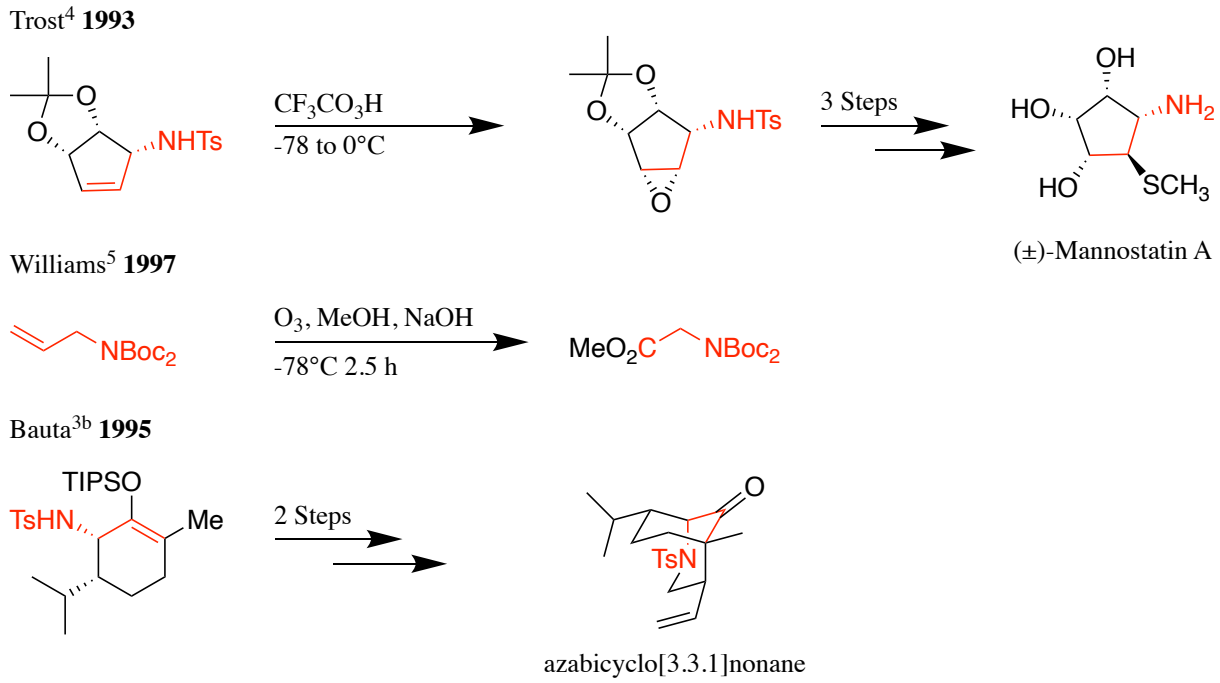

Figure 1.2. Select Examples of Allylic Amines in Synthesis

Trost previously reported that an allylic amine was crucial in a directed epoxidation reaction towards Mannostatin A.[4] Whereas Williams utilized allylic amines in an ozone mediated cleavage reaction, producing amino acids in excellent yields.[5]

Our group aimed to develop an allylic amination reaction on vinylsilanes, an outstanding challenge in the synthetic field. Vinylsilanes are useful reagents for many transformations,[6-8] but few methods exist to functionalize them because of their sensitive reactivity.[7] Even rarer are one-step reactions that meet this goal. Krompiec employs a ruthenium catalyzed reaction to make sulfinated vinylsilanes,[9] whereas Stambuli does allylic C-H acetoxylation (Figure 1.3).[10]

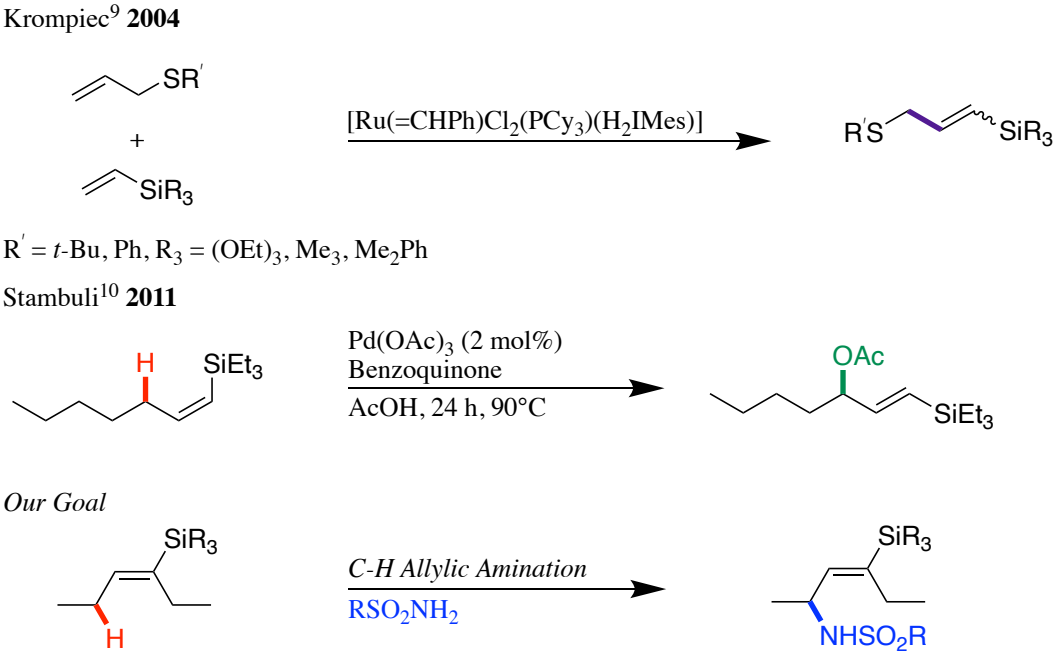

Figure 1.3. Select Examples of One-Step Transformation of Vinylsilanes

In general, the existing one-step methods to functionalize vinylsilanes have significant drawbacks, requiring expensive transition metals or exhibiting limited substrate scopes. There is a need to develop a one-step method that overcomes these obstacles, retains the reactive silane, and enhances the utility of this class of alkenes.

Our group desired to develop an allylic amination involving C-H activation, since it is a more direct route to make allylic amines. A possible hurdle to this endeavor would be chemoselectivity issues concerning vinylsilanes, as reactions could take place at the alkene or directly at the C-Si bond. Even if the silyl group were tolerated in our reaction, our group knew it was important to get selective activation of a single allylic C-H bond. Otherwise, multiple allylic C-H bonds can lead to a mixture of regioisomeric products. Despite these challenges, our group foresaw the value of an allylic C-H amination reaction on electronically diverse alkenes. Aminated vinylsilanes are valuable in some commercial uses,[11-12] but our amination method may serve a greater purpose. Our reaction could be a useful addition to the synthetic chemist's toolbox, a convenient way to functionalize an already important synthon. A C-H allylic amination method of vinylsilanes has not been reported previously.

Our goal for allylic amination on vinylsilanes seemed feasible because of the previous success of C-H allylic amination on aliphatic alkenes (Figure 1.4).

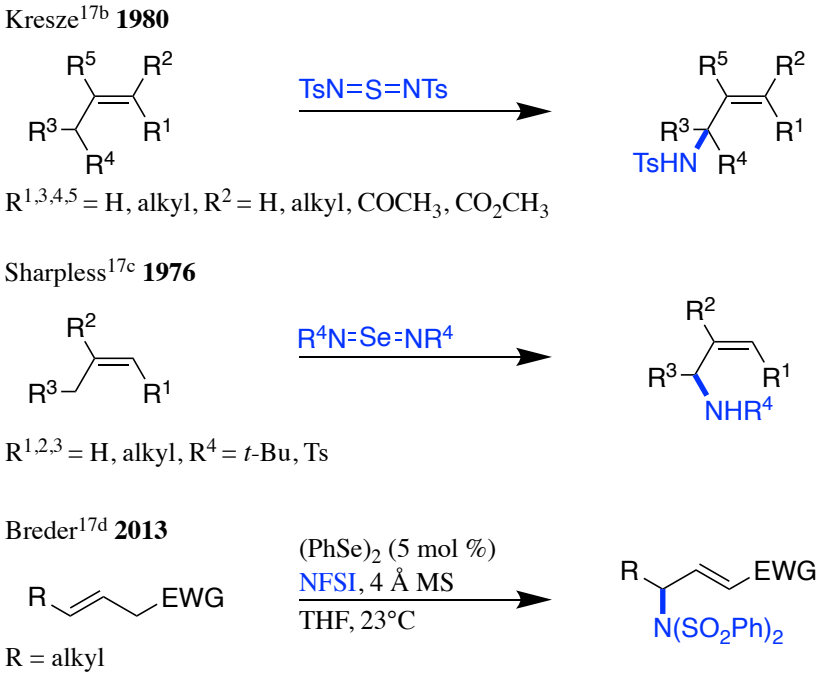

Figure 1.4. Allylic Amination Involving Non-Transition Metals and Nitrene Equivalents

Reported methods primarily required the use of expensive transition metals, such as palladium,[13,14] and in a few cases, rhodium or copper.[15,16] However, an exciting alternative accomplishes C-H allylic amination by means of chalcogen reagents.[17a] Kresze[17b] used a sulfur diimide reagent, whereas Sharpless[17c] relied on in-situ formation of a selenium diimide. Both methods are stoichiometric in selenium or sulfur, which is a drawback since these reagents exhibit toxicity in high amounts. Breder's method[17d] was the first example to use catalytic selenium, but transposition of the double bond occurred in the process to the product. Our group was encouraged by the success of chalcogen-mediated allylic C-H amination, but this technology was not yet applicable to vinylsilanes.

In pursuit of these goals, our group initially reported an allylic C-H amination method on terpenes by means of a novel selenium catalyst, tricyclohexylphosphine selenide (Figure 1.5).[18]

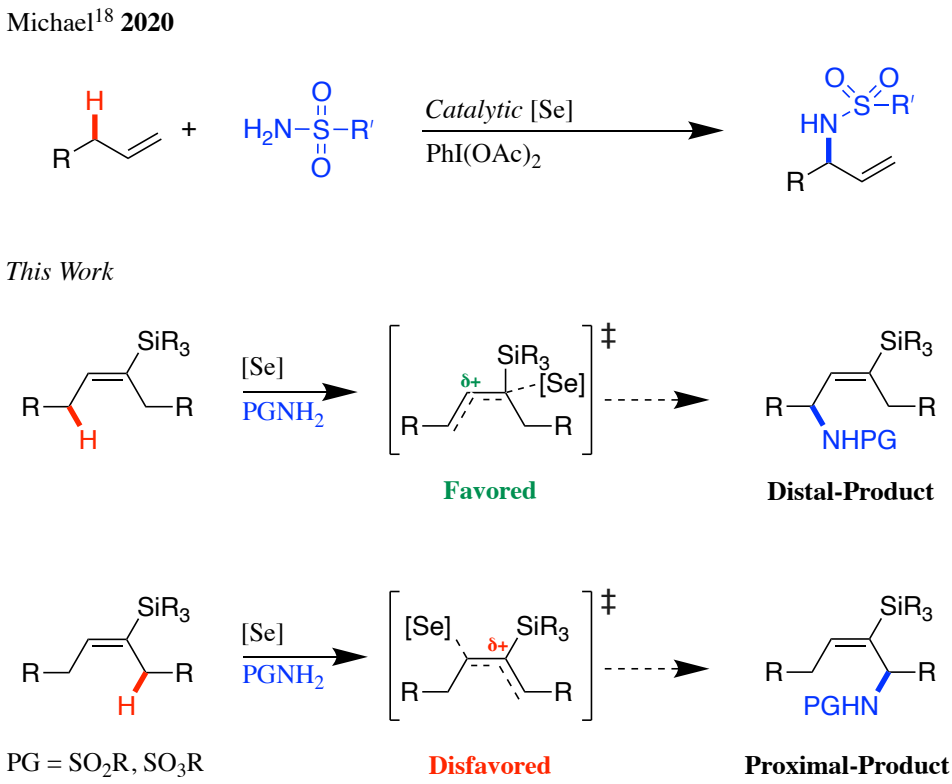

Figure 1.5. Our C-H Allylc Amination Reaction and Proposed Regioselectivity for Vinylsilanes

Wide functional group tolerance was observed, and it was believed that vinylsilanes could be compatible for this protocol. Moreover, we hypothesized that silicon may act as a directing group to promote regioselective abstraction of the distal allylic C-H bond. A polarization in the corresponding ene transition state could be vital to this regioselectivity, perhaps driven by the silicon electronic effects. The distal ene could be favored because positive charge is stabilized by hyperconjugation of the σ Si-C bond into an empty orbital on the β carbon (like a β-silicon effect). Whereas the proximal ene is destabilized by positive charge α to the silane that is unable to be stabilized in the same manner. To our knowledge, regioselectivity for C-H amination in this context has not been predicted or investigated.

Section 2: RESULTS AND DISCUSSION

1.2.1 *Reaction Optimization*

We examined the allylic C-H amination of (*E*)-vinylsilane **1a** with trifluoroethanol sulfonamide ($TfesNH_2$) using conditions developed in our group (Table 1.1).[18]

Table 1.1. Catalyst Screen for Allylic Amination

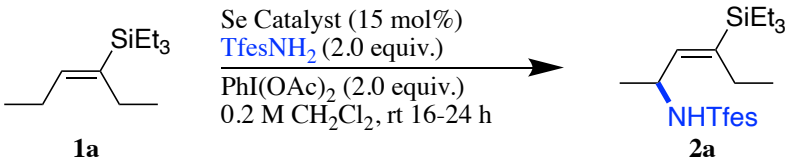

1a **2a**

Entry	Catalyst	%Yield[a]
1	$SePCy_3$	56
2	$SePPh_3$	62[b]
3	$SeP(OPh)_3$	50[b]
4	SeIMe	6
5	SeIMes	0

[a]Yield determined using 1,3-dinitrobenzene as an internal standard. [b]Reaction time was 13 hours.

Fortunately, C-H allylic amination proceeded without competing reaction at the alkene or C-Si bond. The reaction occurred only at the distal site, furnishing 56% yield (Table 1.1, entry 1) of the desired product. *N*-heterocyclic carbene selenides generally underperformed in the reaction, where only a trace amount of product was observed (Table 1.1, entry 4). The triphenylphosphine selenide (Table 1.1, entry 2) catalyst led to 62% of the amination product and was the best performing catalyst tested. Our group was interested in using the same selenium catalyst for amination of terminal and internal vinylsilanes, so we elected to use tricyclohexylphosphine selenide in our method. We next examined the effect of additives (Table 1.2) in the reaction between **1d** and 4-nitrobenzenesulfonamide ($NsNH_2$).

Table 1.2. Effect of Additives on Allylic Amination

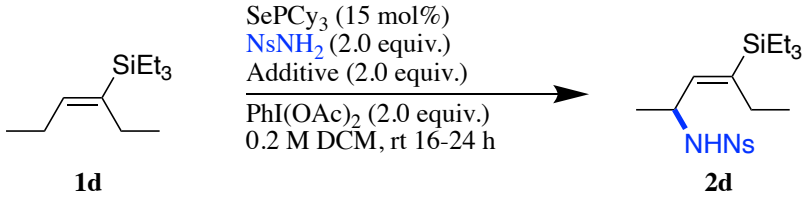

1d **2d**

Entry	Additive	%Yield[a]
1	none	54
2	CaO	32
3	CaO[b]	25
4	$PhCO_2H$	82
5	$4\text{-}NO_2PhCO_2H$	59

[a]Yield determined using 1,3-dinitrobenzene as an internal standard. [b]Reaction was heated at 35°C.

The addition of carboxylic acids generally resulted in increased yields of **2d** (Table 1.2, entries 4 and 5), benzoic acid leading to the best yield of 82%. Oxide bases instead were associated with diminished product yields regardless of heating the reaction (Table 1.2, entry 3).

Section 1.2.2 *Substrate Scope*

Having identified the optimized conditions (Table 1.2, entry 4), the reaction between a range of internal vinylsilanes and $NsNH_2$ was evaluated. While the two products in **2d** are the same regioisomer, the alkene stereochemistry is different among them. In terms of regioselectivity, allylic amination occurred exclusively at the site distal to the silane. The combined yields of the isomers are generally in the 80% range, the exception being the triethoxysilane compound **2g** (Table 1.3).

Table 1.3. Internal Vinylsilane Scope with 4-Nitrobenzenesulfonamide[a]

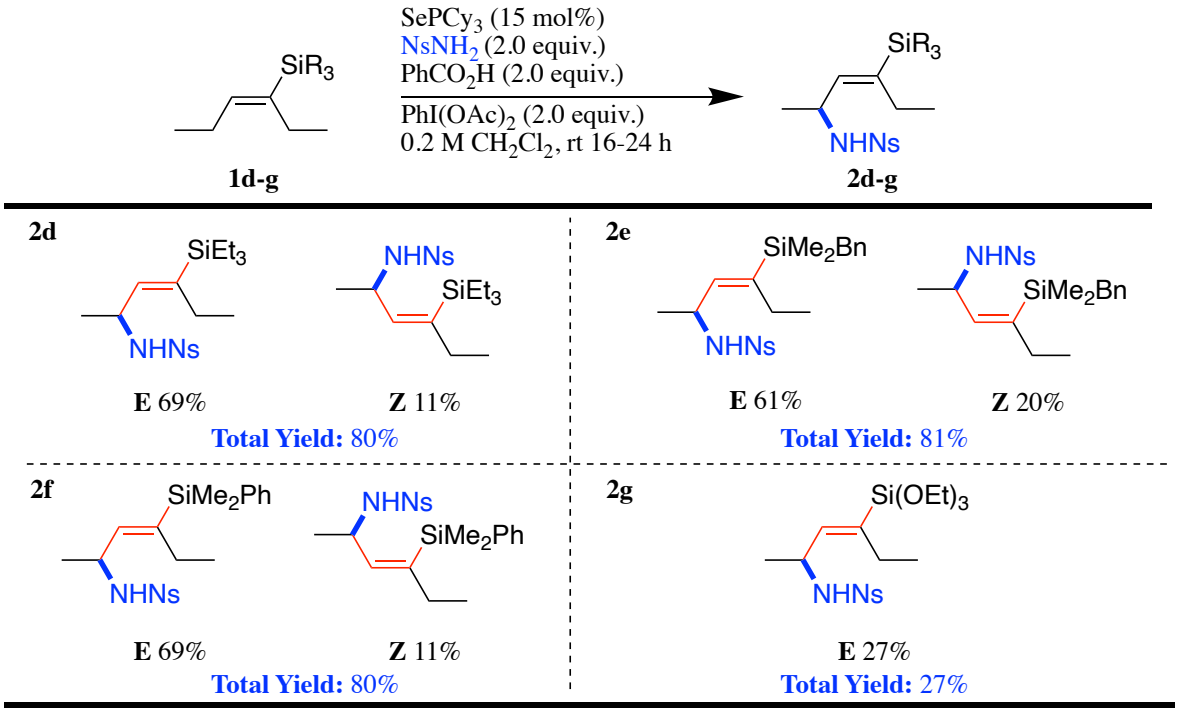

[a]Isolated yields.

The diminished yield for **2g** could be due to the instability of this substrate under the reaction conditions or purification process. Notably, **2e** and **2f** amination products contain silanes that are reactive enough to be used in a Hiyama coupling, an important synthetic transformation.

We previously showed that electron-deficient nitrogen sources were successful in allylic C-H amination,[17] thus we chose to evaluate $TfesNH_2$ in our reaction. When $NsNH_2$ was employed, our internal vinylsilanes led exclusively to the distal amination products. Amination involving $TfesNH_2$ led to yields greater than 75% of the amination products. Interestingly, a minor amount of the proximal amination products was observed for the products **2a** and **2b** (Table 1.4).

Table 1.4. Internal Vinylsilane Scope with Trifluoroethanol Sulfonamide[a]

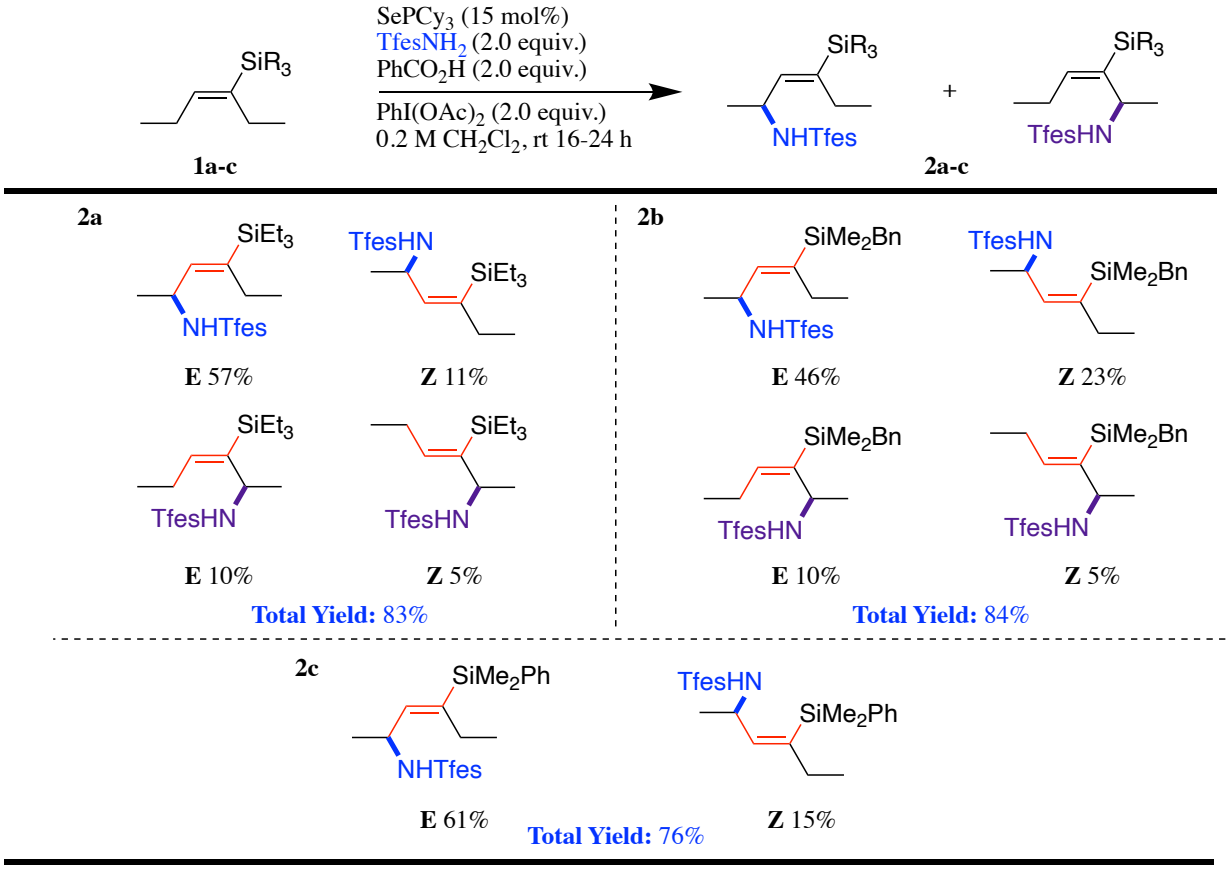

[a]Isolated yields.

We questioned why there was activation of the proximal allylic C-H bond, a computational chemistry study will thus be presented later to elucidate an explanation. We next applied our amination conditions to vinylsilanes containing activated allylic C-H bonds (Figure 1.6).

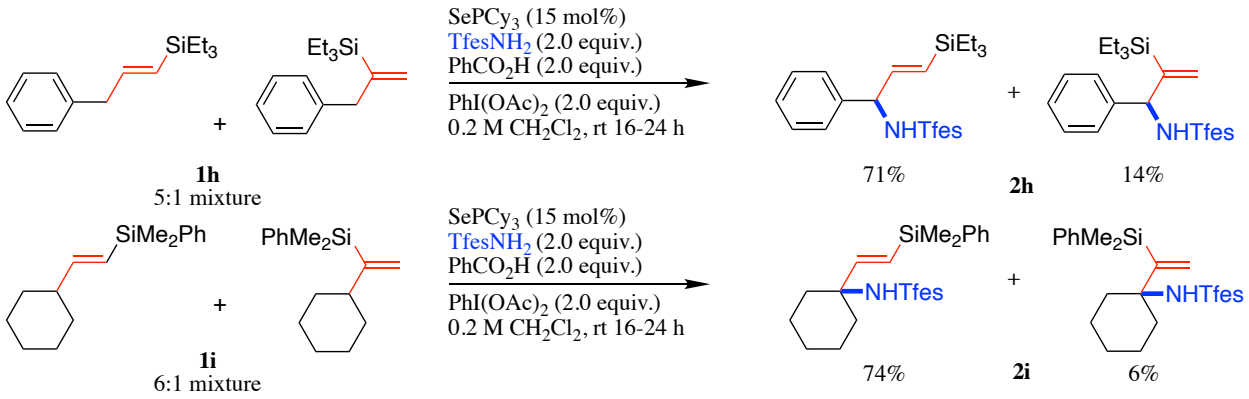

Figure 1.6. Terminal Vinylsilane Scope with Trifluoroethanol Sulfonamide

Activation of benzylic and tertiary C-H bonds was achieved without issue and the isolated yields of the combined isomers were in the 80% range. The substrates were made via hydrosilylation of alkynes, so we could not avoid the generation of the isomeric vinylsilanes.

Section 1.2.3. *Derivatization*

Several transformations were next accomplished with our allylic aminated compounds (Figure 1.7).

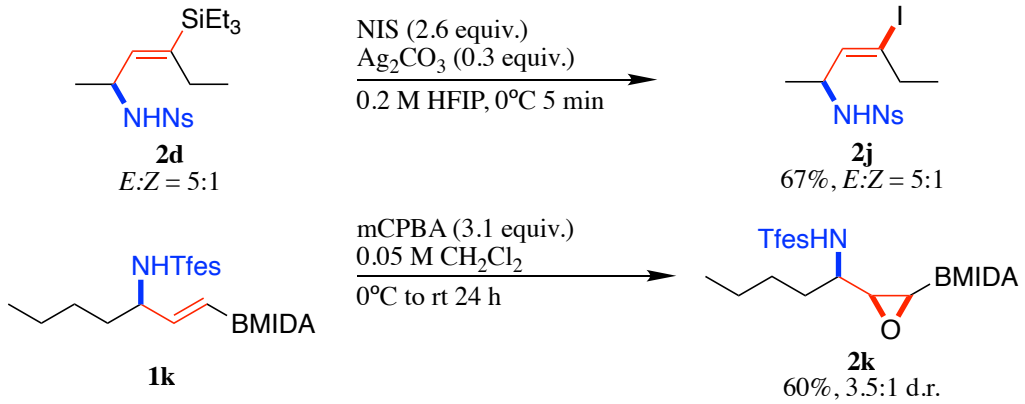

Figure 1.7. Derivatization of Allylic Amination Products

An iododesilylation reaction was demonstrated using a stereo-retentive method, yielding the vinyliodide **2j** in 67% isolated yield. An aminated vinylboronate ester produced by Parker (a collaborator of the project) was subjected to an epoxidation reaction, yielding 60% of the isolated epoxide **2k** in a diastereoselective manner.

Section 1.2.4 *Reaction Scale & Reproducibility*

Our group investigated whether our amination conditions were easily scalable by comparing the isolated yields of amination products from 0.2 and 7 mmol scale reactions. Previously, we demonstrated that our amination reaction on a 0.2 mmol scale led to an 80% isolated yield of the aminated vinylsilane **2d** (Table 1.5, entry 1). The 7 mmol scaled reaction (1.4 g) gave an average isolated yield of 46% over 2 attempts.

Table 1.5. Evaluation of Reaction Scale on Allylic Amination

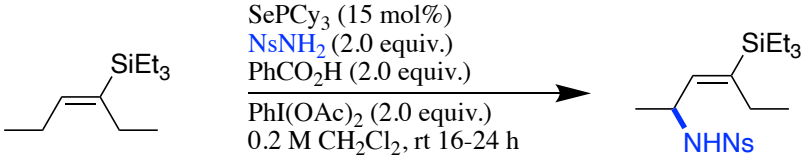

1 **2d**

Entry	Quantity of **1** (mmol)	%Yield[a]
1	0.2	80
2	7	47
3	7	45

[a]Isolated yield.

The diminished yield could be attributed to the fact that the amination reaction is heterogeneous. Our experimental observations suggest that the double allylic amination product could have accounted for the missing mass balance.

Section 3: CONCLUSION

A reaction was developed and applicable to C-H allylic amination on internal vinylsilanes. A range of silanes on the alkene was compatible with this method and the isolated yields were generally greater than 75%. When $NsNH_2$ was employed as the nucleophile, activation of the distal allylic C-H bond was observed exclusively. In contrast, the use of $TfesNH_2$ resulted in the generation of some of the proximal amination product. We demonstrated that our optimized conditions were successful on vinylsilanes containing benzylic and tertiary allylic C-H bonds. Derivatization of the aminated products was achieved by means of an iododesilylation and epoxidation reaction. The amination reaction was accomplished on large scale (1.4 g) and reproducible to obtain a modest yield of the aminated product.

Section 4: EXPERIMENTAL

1.4.1. *General Procedures and Materials*

All reactions were performed under a nitrogen atmosphere using oven-dried or flame-dried glassware, unless otherwise indicated. Deuterated solvents ($CDCl_3$, DMSO-d^6) were obtained from Cambridge Isotope Laboratories, Inc. THF, CH_2Cl_2, ether, benzene, and toluene were degassed and dried by passing through columns of neutral alumina. Ethyl acetate (EtOAc), hexanes, and ether (Et_2O) were obtained from Fisher Scientific or Sigma Aldrich and used without further purification. Reagents were purchased from Sigma Aldrich, Tokyo Chemical Industry, Fisher Scientific, Alfa Aesar, Oakwood Chemicals, Strem Chemicals and used without further

purification, unless otherwise indicated. Infrared spectra were acquired using a Perkin Elmer Spectrum RX I spectrometer. Mass spectra were acquired using a Bruker Esquire 1100 Liquid Chromatograph-Ion Trap Mass Spectrometer. Column chromatography was performed using silica gel (Whatman, 60 Å, 230-400 mesh). NMR spectra were recorded on a Bruker AV-300, AV-301, DRX-499, or AV-500 spectrometer. ^{1}H NMR chemical shifts (δ) are reported in parts per million (ppm) and are referenced to residual solvent signal of $CHCl_3$ (7.26 ppm) or DMSO-d^6 (2.50 ppm). ^{13}C NMR chemical shifts (δ) are reported in parts per million (ppm) relative to the carbon resonance of $CDCl_3$ (77.26 ppm) or DMSO-d^6 (39.52 ppm). Melting points were obtained on a MEL-TEMP melting point apparatus and are uncorrected.

1.4.2. *Synthesis of Selenium Catalysts and Starting Materials*

Selenium catalysts and trifluoroethanol sulfonamide were synthesized according to literature procedure and the spectroscopic data were consistent with the reported values.[18] Starting material alkenes and sulfonamides are purchased from commercial sources and used without further purification, unless otherwise indicated. Internal vinylsilanes and terminal vinylsilanes were synthesized according to a general procedure[19] and the spectroscopic data were consistent with the literature values.[20]

Section 1.4.3. *General Procedure for Selenium Catalyzed Allylic Amination*

An oven-dried 4-dram vial equipped with a stir bar was charged with tricyclohexylphosphine selenide (0.03 mmol, 15 mol %). Sulfonamide (0.4 mmol), benzoic acid (0.4 mmol), and

vinylsilane (0.2 mmol) were added to the vial in that order. Dichloromethane (1 mL) was added followed by diacetoxyiodobenzene (0.4 mmol). The solution was flushed with nitrogen and the vial sealed with a Teflon cap. The solution was stirred at room temperature until reaction completion, as judged by thin layer chromatography, typically 16-24 hours. The crude reaction mixture was then diluted with 30 mL ethyl acetate. The organic layer was washed with 3 x 30 mL saturated $NaHCO_3$, 1 x 30 mL H_2O, and 1 x 30 mL brine. The aqueous layers were extracted 1 x 30 mL ethyl acetate. All combined organic layers were dried with $MgSO_4$ and concentrated under vacuum. The crude reaction mixture was separated using silica gel chromatography with an ethyl acetate/hexane mixture to afford the desired amination product.

Section 1.4.4. *Characterization of Products*

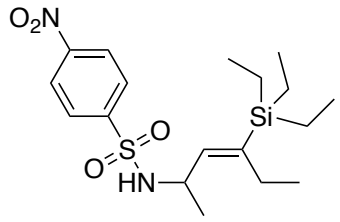

2d. Prepared according to the general procedure and purified by silica gel chromatography to afford the product as a white crystalline solid (63.8 mg, 80% yield, *E*:*Z* = 6:1). **^{1}H NMR** (300 MHz, DMSO-d_6): δ 8.37 (d, *J* = 8.8 Hz, 2 H), 8.25 (d, *J* = 8.2 Hz, 1 H), 7.99 (d, *J* = 8.8 Hz, 2 H), 5.26 (d, *J* = 8.9 Hz, 1 H), 4.26 - 4.14 (m, 1 H), 2.01 – 1.75 (m, 2 H), 1.10 (d, *J* = 6.7 Hz, 3 H), 0.78 (t, *J* = 7.4 Hz, 3 H), 0.71 (t, *J* = 7.8 Hz, 9 H), 0.37 – 0.28 (m, 6 H). **^{13}C NMR** (126 MHz, DMSO-d_6): δ 149.29, 147.75, 141.59, 138.52, 127.99, 124.40, 47.13, 22.66, 22.13, 14.46, 7.15, 2.41. **IR** (thin film): 3271, 3093, 2958, 2914, 2869, 1601, 1529, 1456, 1410, 1342, 1307, 1163, 1088, 1061,

999, 848, 732, 677, 615, 560, 457 cm^{-1}. **MS** (ESI, negative mode): 397.7 ($M\text{-}H^+$). **Melting Point**: 82 - 86 °C.

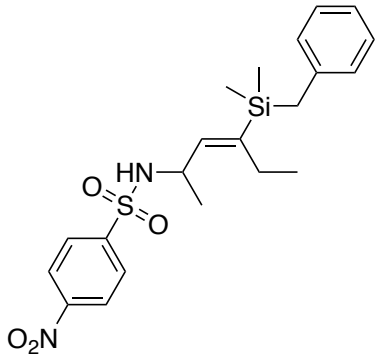

2e. Prepared according to the general procedure and purified by silica gel chromatography to afford the product as a yellow crystalline solid (71.4 mg, 81% yield, *E*:*Z* = 3:1). **^{1}H NMR** (300 MHz, DMSO-d_6) δ: 8.38 (d, *J* = 8.8 Hz, 2 H), 8.19 (d, *J* = 8.2 Hz, 1 H), 7.99 (d, *J* = 8.8 Hz, 2 H), 7.13 (t, *J* = 7.8 Hz, 2 H), 7.00 (t, *J* = 6.9 Hz , 1 H), 6.84 (d, *J* = 7.2 Hz, 2 H), 5.14 (d, *J* = 8.8 Hz, 1 H), 4.24 – 4.11 (m, 1 H), 2.08 - 1.90 (m, 2 H), 1.87 (s, 2 H), 1.06 (d, *J* = 6.5 Hz, 3 H), 0.79 (t, *J* = 7.4 Hz, 3 H), -0.22 (s, 3 H), -0.33 (s, 3 H). **^{13}C NMR** (126 MHz, DMSO-d_6) δ: 149.33, 147.80, 141.07, 140.03, 139.36, 128.23, 128.01, 127.95, 124.33, 123.96, 47.20, 24.62, 22.05, 21.99, 14.59, -3.91, -4.09. **IR** (thin film): 3279, 3096, 2967, 2915, 1603, 1526, 1490, 1448, 1412, 1345, 1309, 1247, 1195, 1159, 1087, 1056, 989, 927, 829, 736, 695, 617, 566, 468 cm^{-1}. **MS** (ESI, negative mode): 431.3 ($M\text{-}H^+$). **Melting Point:** 61 - 66 °C.

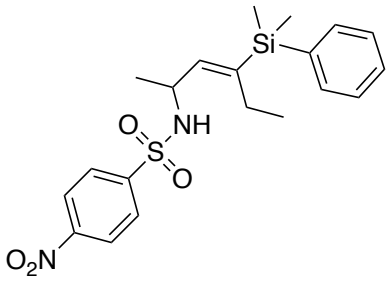

2f. Prepared according to the general procedure and purified by silica gel chromatography to afford the product as an opaque/white crystalline solid (66.4 mg, 80% yield, *E*:*Z* = 6:1). **^{1}H NMR** (300 MHz, DMSO-d_6) δ: 8.37 (d, *J* = 8.8 Hz, 2 H), 8.25 (d, *J* = 8.2 Hz, 1 H), 7.99 (d, *J* = 9.0 Hz, 2 H), 7.37 – 7.22 (m, 5 H), 5.34 (d, *J* = 8.9 Hz, 1 H), 4.27 – 4.12 (m, 1 H), 2.03 – 1.72 (m, 2 H), 1.11 (d, *J* = 6.7 Hz, 3 H), 0.66 (t, *J* = 7.4 Hz, 3 H), 0.11 (s, 3 H), 0.06 (s, 3 H). **^{13}C NMR** (126 MHz, DMSO-d_6) δ: 149.27, 147.71, 141.61, 140.03, 137.53, 133.53, 128.99, 128.06, 127.64, 124.33, 47.21, 22.27, 22.01, 14.53, -3.00, -3.36. **IR** (thin film): 3266, 3107, 3072, 2958, 2924, 2844, 1606, 1527, 1447, 1424, 1344, 1304, 1247, 1162, 1105, 1088, 1059, 991, 922, 848, 814, 768, 734, 700, 677, 614, 563, 460 cm^{-1}. **MS** (ESI, negative mode): 417.3 ($M-H^+$). **Melting Point:** 89 - 93 °C.

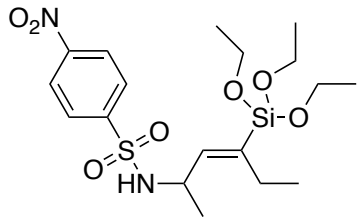

2g. Prepared according to the general procedure and purified by silica gel chromatography to afford the product as a clear oil (25.4 mg, 27% yield). **^{1}H NMR** (300 MHz, DMSO-d_6) δ: 8.37 (d, *J* = 8.5 Hz, 2 H), 8.25 (d, *J* = 8.2 Hz, 1 H), 7.98 (d, *J* = 8.5 Hz, 2 H), 5.54 (d, *J* = 8.8 Hz, 1 H), 4.25 – 4.11 (m, 1 H), 3.55 (q, *J* = 6.9 Hz, 6 H), 2.05 – 1.78 (m, 2 H), 1.10 – 1.04 (m, 12 H), 0.83 (t, *J* = 7.2 Hz, 3H). **^{13}C NMR** (126 MHz, DMSO-d_6) δ: 149.27, 147.47, 144.28, 133.85, 127.99, 124.38, 57.76, 46.88, 22.04, 21.59, 17.98, 14.00. **IR** (thin film): 3447, 2972, 2917, 1635, 1530, 1348, 1304, 1160, 1072, 951, 851, 774, 730, 686, 614, 570, 531, 465 cm^{-1}. **MS** (ESI, negative mode): 445.4 ($M-H^+$).

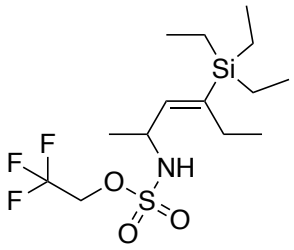

2a. Prepared according to the general procedure and purified by silica 5el chromatography to afford the product as a clear oil (63.6 mg, 83% yield, 6:1 mixture of regioisomers, *E:Z* = 4:1). **^{1}H NMR** (300 MHz, DMSO-d_6) δ: 8.47 (d, *J* = 7.1 Hz, 1 H), 5.56 (d, *J* = 8.8 Hz, 1 H), 4.72 – 4.45 (m, 2 H), 4.36 – 4.18 (m, 1 H), 2.22 – 1.93 (m, 2H), 1.18 (d, *J* = 6.3 Hz, 3 H), 0.98 – 0.80 (m, 12 H), 0.60 – 0.51 (m, 6 H). **^{13}C NMR** (126 MHz, DMSO-d_6) δ: 141.27, 139.07, 122.88 (q, *J* = 278.4 Hz), 63.87 (q, *J* = 36.1 Hz), 47.73, 22.17, 21.95, 14.56, 7.17, 2.45. **IR** (thin film): 3550, 3309, 2957, 2881, 1617, 1453, 1420, 1365, 1283, 1178, 1047, 1003, 959, 920, 899, 855, 800, 723, 663, 597, 558, 514 cm^{-1}. **MS** (ESI, negative mode): 374.2 (M-H^{+}).

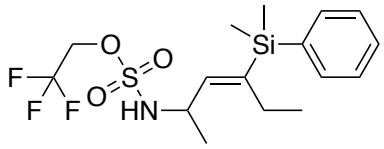

2c. Prepared according to the general procedure and purified by silica gel chromatography to afford the product as a clear oil (60.7 mg, 76% yield, *E:Z* = 4:1). **^{1}H NMR** (300 MHz, DMSO-d_6) δ: 8.49 (d, *J* = 7.3 Hz, 1 H), 7.55 – 7.44 (m, 3H), 7.38 – 7.31 (m, 2 H), 5.65 (d, *J* = 9.0 Hz, 1 H), 4.69 – 4.42 (m, 2 H), 4.35 – 4.21 (m, 1 H), 2.23 – 2.00 (m, 2 H), 1.19 (d, *J* = 6.7 Hz, 3 H), 0.81 (t, *J* = 7.6 Hz, 3 H), 0.32 (s, 6 H). **^{13}C NMR** (126 MHz, DMSO-d_6) δ: 141.41, 140.81, 137.75, 133.72, 129.06, 127.78, 122.88 (q, *J* = 272.8 Hz), 63.87 (q, *J* = 35.1 Hz), 47.83, 22.13, 21.69, 14.65, -2.96, -2.99.

IR (thin film): 3292, 3059, 2955, 2920, 2862, 1605, 1523, 1424, 1360, 1285, 1180, 1052, 1000, 959, 808, 773, 732, 697, 610, 558, 470 cm^{-1}. **MS** (ESI, negative mode): 394.2 ($M-H^+$).

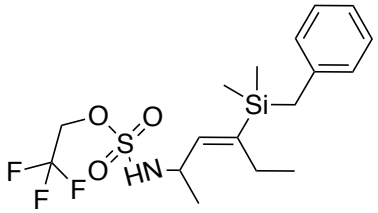

2b. Prepared according to the general procedure and purified by silica gel chromatography to afford the product as a clear oil (69.1 mg, 84% yield, 6:1 mixture of regioisomers, *E:Z* = 2:1). **^{1}H NMR** (300 MHz, DMSO-d_6) δ: 8.45 (d, *J* = 7.4 Hz, 1 H, E), 8.50 (d, *J* = 7.3 Hz, 1 H, Z), 7. 17 (m, 2 H, E and Z), 7.03 (t, *J* = 8.0 Hz, 3 H, Z), 6.98 (t, *J* = 7.5 Hz, 3 H, E), 5.85 (d, *J* = 9.7 Hz, 1 H, Z), 5.53 (d, *J* = 8.9 Hz, 1 H, E), 4.75 – 4.45 (m, 4H, E and Z), 4.32 – 4.21 (m, 1 H, E), 4.21 – 4.09 (m, 1 H, Z), 2.22 (s, 2H, Z), 2.12 (s, 2 H, E), 2.09 (q, *J* = 5.4 Hz, 2 H, E), 1.98 (q, *J* = 7.3 Hz) 1.15 (d, *J* = 6.7 Hz, 3 H, E), 1.13 (d, *J* = 6.2 Hz, 3 H, Z), 0.96 – 0.84 (m, 6 H, E and Z), 0.08 (s, 3H, Z), 0.07 (s, 3H, Z), 0.01 (s, 3 H, E), -0.01 (s, 3H, E). **^{13}C NMR** (126 MHz, DMSO-d_6) δ: 141.82, 140.75, 128.07, 127.95, 124.05, 123.92, 122.74 (q, *J* = 257.3 Hz), 63.90 (q, *J* = 35.9 Hz), 47.78, 24.73, 22.02, 21.59, 14.61, -3.70, -3.82. **IR** (thin film): 3305, 3062, 3028, 2962, 2918, 1597, 1491, 1420, 1364, 1281, 1248, 1176, 1055, 1000, 961, 928, 900, 828, 756, 701, 657, 557, 475 cm^{-1}. **MS** (ESI, negative mode): 408.6 ($M-H^+$).

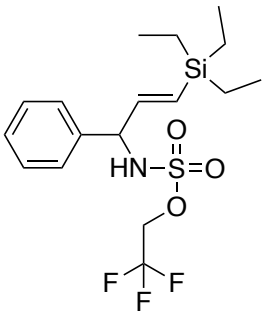

2h. Prepared according to the general procedure and purified by silica gel chromatography to afford the product as a clear oil (70.3 mg, 85% yield, isolated as a 5:1 mixture of silane regioisomers present in the starting material). **^{1}H NMR** (300 MHz, DMSO-d_6) δ: 9.16 (d, J = 8.6 Hz, 1 H), 7.41 – 7.25 (m, 5 H), 6.14 (dd, J = 18.7, 5.7 Hz, 1 H), 5.83 (d, J = 18.9 Hz, 1 H), 5.08 – 4.97 (m, 1 H), 4.58 – 4.32 (m, 2 H), 0.88 (t, J = 7.9 Hz, 9 H), 0.53 (q, J = 7.7 Hz, 6 H). **^{13}C NMR** (126 MHz, DMSO-d_6) δ: 145.59, 140.11, 128.52, 127.62, 127.02, 126.68, 122.62 (q, J = 279.0 Hz), 64.01 (q, J = 36.5 Hz), 61.92, 7.13, 2.84. **IR** (thin film): 3432, 3302, 2947, 2905, 2873, 1626, 1453, 1417, 1369, 1286, 1181, 1050, 958, 856, 772, 721, 696, 561 cm^{-1}. **MS** (ESI, negative mode): 408.3 (M-H^{+}).

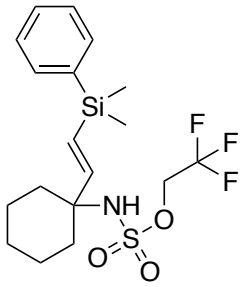

2i. Prepared according to the general procedure and purified by silica gel chromatography to afford the product as a clear oil (67.2 mg, 80% yield, isolated as a 13:1 mixture of silane regioisomers

while ratio in the starting material was 6:1). **^{1}H NMR** (300 MHz, DMSO-d_6) δ: 8.12 (s, 1 H), 7.54 – 7.46 (m, 2 H), 7.38 – 7.31 (m, 3 H), 6.14 (d, *J* = 18.9 Hz, 1 H), 5.95 (d, *J* = 18.9 Hz, 1 H), 4.55 (q, *J* = 8.6 Hz, 2 H), 1.90 – 1.75 (m, 2 H), 1.69 – 1.21 (m, 8 H), 0.30 (s, 6 H). **^{13}C NMR** (126 MHz, DMSO-d_6) δ: 150.99, 138.13, 133.58, 129.02, 127.77, 126.16, 122.86 (q, *J* = 278.5 Hz), 63.77 (q, *J* = 36.8 Hz), 59.97, 34.58, 24.85, 21.44, -2.74. **IR** (thin film): 3292, 3060, 2939, 2850, 1613, 1453, 1420, 1365, 1282, 1249, 1177, 1111, 1050, 995, 956, 917, 901, 846, 829, 790, 730, 697, 658, 608, 586, 559, 465 cm^{-1}. **MS** (ESI, negative mode): 420.2 ($M-H^+$).

Iododesilylation of internal vinylsilane. By using a slightly modified preparation outlined by Vilarrasa and co-workers,[21] iododesilylation of an internal vinylsilane was achieved.

To an oven-dried 4-dram vial charged with a stir bar, **2d** (0.0798 g, 0.2 mmol) was added followed by distilled hexafluoroisopropanol (1 mL). The vial was protected from light with foil and the solution was stirred at room temperature for 10 min, then cooled to 0 °C for 10 min. At 0 °C, Ag_2CO_3 (0.0184 g, 0.0667 mmol) was added and then *N*-iodosuccinimide (0.1175 g, 0.522 mmol) in one portion. The reaction mixture was stirred at 0 °C for 5 minutes and then quenched with cold H_2O. The suspension was diluted with 30 mL dichloromethane and the organic layer was extracted with 30 mL water. The aqueous layer was next extracted with 2 x 30 mL dichloromethane and the combined organic layers were dried with magnesium sulfate and concentrated. Separation by silica gel chromatography with ethyl acetate/hexane mixtures from 5% to 30 % afforded a white crystalline solid **2j** (0.0548 g, 67%),

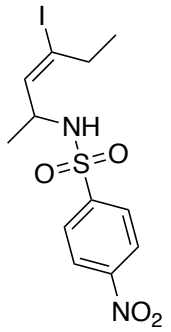

2j. Prepared according to the above procedure and purified by silica gel chromatography to afford the product as a white crystalline solid (54.8 mg, 67% yield, *E:Z* = 5:1). **^{1}H NMR** (300 MHz, DMSO-d_6) δ: 8.41 (d, *J* = 8.7 Hz, 2 H), 8.36 (d, *J* = 7.9 Hz, 1 H), 8.00 (d, *J* = 8.7 Hz, 2 H), 5.23 (d, *J* = 8.2 Hz, 1 H), 3.98 – 3.84 (m, 1 H), 2.27 – 2.06 (m, 2 H), 1.08 (d, *J* = 6.8 Hz, 3 H), 0.70 (t, *J* = 7.2 Hz, 3 H). **^{13}C NMR** (126 MHz, DMSO-d_6) δ: 149.49, 147.08, 134.60, 128.28, 124.38, 110.39, 55.83, 37.69, 20.73, 14.07. **IR** (thin film): 3580, 3274, 3095, 2961, 2924, 2872, 1642, 1605, 1523, 1448, 1418, 1344, 1307, 1158, 1076, 986, 904, 852, 733, 681, 614, 561, 464 cm^{-1}. **MS** (ESI, negative mode): 409.2 ($M-H^+$). **Melting Point**: 106 - 108 °C.

Epoxidation of BMIDA aminated substrate. A preparation developed by Burke et al. was slightly modified to provide an epoxy MIDA boronate product.[22]

To an oven-dried 4-dram vial charged with a stir bar, **1k** (0.0867 g, 0.201 mmol) was added followed by dichloromethane (4 mL). The vial was cooled to 0 °C for 15 min and then mCPBA (0.1434 g, 3.174 mmol, 77% pure) was added and capped with a Teflon cap. The vial was allowed to stir at room temperature for 24 h. The mixture was diluted with ethyl acetate (30 mL) and the organic layer was extracted with saturated aq $NaHCO_3$ (1 x 30 mL). The aqueous layer was

extracted with ethyl acetate (2 x 30 mL). The organic phases were combined and washed with sodium sulfite (2 x 30 mL), H_2O (1 x 30 mL), and brine (1 x 30 mL). The organic fractions were dried over $MgSO_4$, filtered, and concentrated under vacuum to provide **2k** as a white crystalline solid (54.2 mg, 60%).

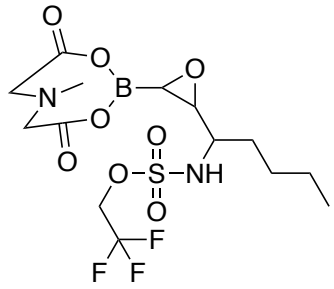

2k. Prepared according to the above procedure and purified by silica gel chromatography to afford the product as a white crystalline solid (54.2 mg, 60% yield, dr = 3.5:1). **^{1}H NMR** (300 MHz, DMSO-d_6) δ: 8.61 (d, *J* = 8.3 Hz, 1 H), 4.65 (q, *J* = 8.5 Hz, 2 H), 4.32 (d, *J* = 17.0 Hz, 1 H), 4.20 (d, *J* = 17.0 Hz, 1 H), 4.08 (d, *J* = 17.2 Hz, 1 H), 3.93 (d, *J* = 17.0 Hz, 1 H), 3.08 – 2.95 (m, 4 H), 2.79 (dd, *J* = 7.0, 2.9 Hz, 1 H), 2.28 (d, *J* = 2.8 Hz, 1 H), 1.85 – 1.11 (m, 6 H), 0.86 (t, *J* = 6.8 Hz, 3 H). **^{13}C NMR** (126 MHz, DMSO-d_6) δ: 169.33, 168.46, 122.86 (q, *J* = 277.7 Hz), 64.10 (q, *J* = 35.2 Hz), 62.05, 61.85, 57.74, 57.03, 47.53, 46.43, 31.80, 27.15, 21.99, 13.78. **IR** (thin film): 3526, 3275, 3013, 2956, 2922, 2865, 1765, 1451, 1343, 1280, 1177, 1041, 955, 892, 858, 801, 733, 653, 590, 562 cm^{-1}. **MS** (ESI, negative mode): 445.0 ($M-H^+$). **Melting Point**: 158 -162 °C.

REFERENCES FOR CHAPTER 1

[1] (a) Hili, R.; Yudin, A. K. *Nat. Chem. Biol.* **2006,** *2,* 284-287. (b) Sharpe, L. G.; Pickworth, W. B. *Brain. Res. Bull.* **1985,** *3,* 329-333. (c) Vitaku, E.; Smith, D. T.; Njardarson, J. T. *J. Med. Chem.* **2014,** *57,* 10257−10274.

[2] (a) Fuerst, S.; Hosztafi, S.; Friedmann, T. *Curr. Med. Chem.* **1995,** *1,* 423–440. (b) Richter, M. F.; Drown, B. S.; Riley, A. P.; Garcia, A.; Shirai, T.; Svec, R. L.; Hergenrother, P. J. *Nature,* **2017,** *545,* 299−304.

[3] (a) Johannsen, M.; Jørgensen, K. A. *Chem. Rev.* **1998,** *98,* 1689-1708. (b) Magnus, P.; Lacour, J.; Coldham, I.; Mugrage, B.; Bauta, W. B. *Tetrahedron* **1995,** *51,* 11087-11110. (c) Skoda, E. M.; Davis, G. C.; Wipf, P. *Org. Process. Res. Dev.* **2012,** *16,* 26-34. (d) Weiner, B.; Baeza, A.; Jerphagnon, T.; Feringa, B. L. *J. Am. Chem. Soc.* **2009,** *131,* 9473−9474.

[4] Trost, B. M.; Vranken, D. L. *J. Am. Chem. Soc.* **1993,** *115,* 444-458.

[5] Bower, J. F.; Jumnah, R.; Williams, A. C.; Williams, J. M. J. *J. Chem. Soc. Perkin Trans.* **1997,** *1,* 1411-1420.

[6] Fristad, W. E.; Dime, D. S.; Bailey, T. R.; Paquette, L. A. *Tetrahedron Lett.* **1979,** *22,* 1999.

[7] Langkopf, E.; Schinzer, D. *Chem. Rev.* **1995,** *95,* 1375-1408.

[8] (a) Kim, J.; Hewitt, G.; Carroll, P.; Sieburth, S. M.; *J. Org. Chem.* **2005,** *70,* 5781-5789; (b) Franz, A. K.; Wilson, S. O. *J. Med. Chem.* **2012,** *55,* 388-405. (c) Meanwell, N. A. *J. Med. Chem.* **2011,** *54,* 2529-2591.

[9] Marciniec, B.; Chadyniak, D.; Krompiec, S. *J. Mol. Cat. A. Chem.* **2004,** *224,* 111-116.

[10] Check, C. T.; Henderson, W. H.; Wray, B. C.; Vanden Eynden, M. J.; Stambuli, J. P. *J. Am. Chem. Soc.* **2011,** *133,* 18503-18505.

[11] L'Oreal, Fr. Lightening and/or Dyeing of Human Keratin Fibers by Means of a Composition Comprising a Particulate Aminosilicone Compound. WO 2009056779 A2, May 7, 2009.

[12] Switzer, J. R.; Ethier, A. L.; Hart, E. C.; Flack, K. M.; Rumple, A. C.; Donaldson, J. C.; Bembry, A. T.; Scott, O. M.; Biddinger, E. J.; Talreja, M.; Song, M.-G.; Pollet, P.; Eckert, C. A.; Liotta, C. L. *ChemSusChem.* **2014,** *7,* 299-307.

[13] Godleski, S. A. In Comprehensive Organic Synthesis, 1st ed. Semmelhack, M. F., Ed.; Pergamon Press: New York, 1991; Vol. 4; pp 585.

[14] Trost, B. M.; Vranken, D. L. *J. Am. Chem. Soc.* **1993,** *115,* 444-458.

[15] Harris, R. J.; Park, J.; Nelson, T. A. F.; Iqbal, N.; Salgueiro, D. C.; Bacsa, J.; MacBeth, C. E.; Baik, M.-H.; Blakey, S. B. *J. Am. Chem. Soc.* **2020,** *142,* 5842-5851.

[16] Baruah, J. B.; Samuelson, A. G. *Tetrahedron,* **1991,** *47,* 9449.

[17] There are few reports discussing metal-free allylic C-H amination. (a) Singh, F. V.; Wirth, T. *Catal. Sci. Technol.* **2019,** *9,* 1073-1091. (b) Bussas, R.; Kresze, G. *Ann. Chem.* **1980,** 629-649. (c) Sharpless, K. B.; Hori, T.; Truesdale, L. K.; Dietrich, C. O. *J. Am. Chem. Soc.* **1976,** *98,* 269-271. (d) Trenner, J.; Depken, C.; Weber, T.; Breder, A. *Angew. Chem. Int. Ed.* **2013,** *52,* 8952-8956.

[18] Teh, W. P.; Obenschain, D. C.; Black, B. M.; Mi-chael, F. E. *J. Am. Chem. Soc.* **2020,** *142,* 16716-16722.

[19] Chauhan, M.; Hauck, B. J.; Keller, L. P.; Boudjouk, P. *J. Organomet. Chem.* **2002,** *645,* 1- 13.

[20] Spectral data for internal vinylsilanes (a) Nakamura, S.; Uchiyama, M.; Ohwada, T. *J. Am. Chem. Soc.* **2004,** *36,* 11146-11147. (b) Wu, S.; Zhang, Y.; Jiang, H.; Ding, N.;

Wang, Y.; Su, Q.; Zhang, H.; Wu, L.; Yang, W. *Tetrahdedon Lett.* **2020,** *61,* 152053-152057.

[21] Sidera, M.; Costa, A. M.; Vilarrasa, J. *Org. Lett.* **2011,** *13,* 4934-4937.

[22] Udo; B. E.; Gillis, E. P.; Burke, M. D. *Tetrahedron,* **2009,** *65,* 3130-3138.

Chapter 2. DFT REACTION COORDINATE OF ALLYLIC C-H AMINATION OF VINYLSILANES

Section 1: INTRODUCTION

We successfully developed a regioselective amination of vinylsilanes, but we questioned the cause for selectivity of allylic C-H bonds. Like allylic amination, allylic hydroxylation is a selenium mediated transformation that oxidizes the allylic position. This transformation proceeds through an ene step[1] and [2,3]-sigmatropic rearrangement (Figure 2.1).[2]

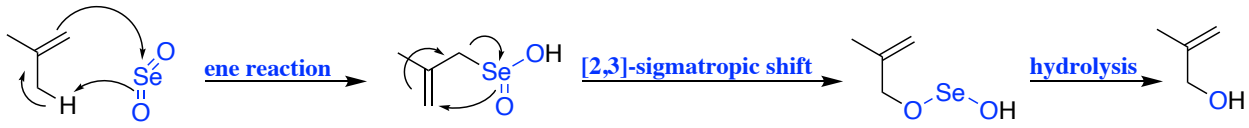

Figure 2.1. Reaction Mechanism of Allylic Hydroxylation

Our group values the insights gathered from computational chemistry and its potential to inform us on the mechanism of allylic C-H amination. Unfortunately, computational work on the fundamental steps of the allylic amination reaction is minimal. Our group proposed a reaction mechanism like allylic hydroxylation for our allylic amination reaction (Figure 2.2). Our group had only elucidated an ene transition state for the propene molecule, mediated by a selenium diimide species.[3]

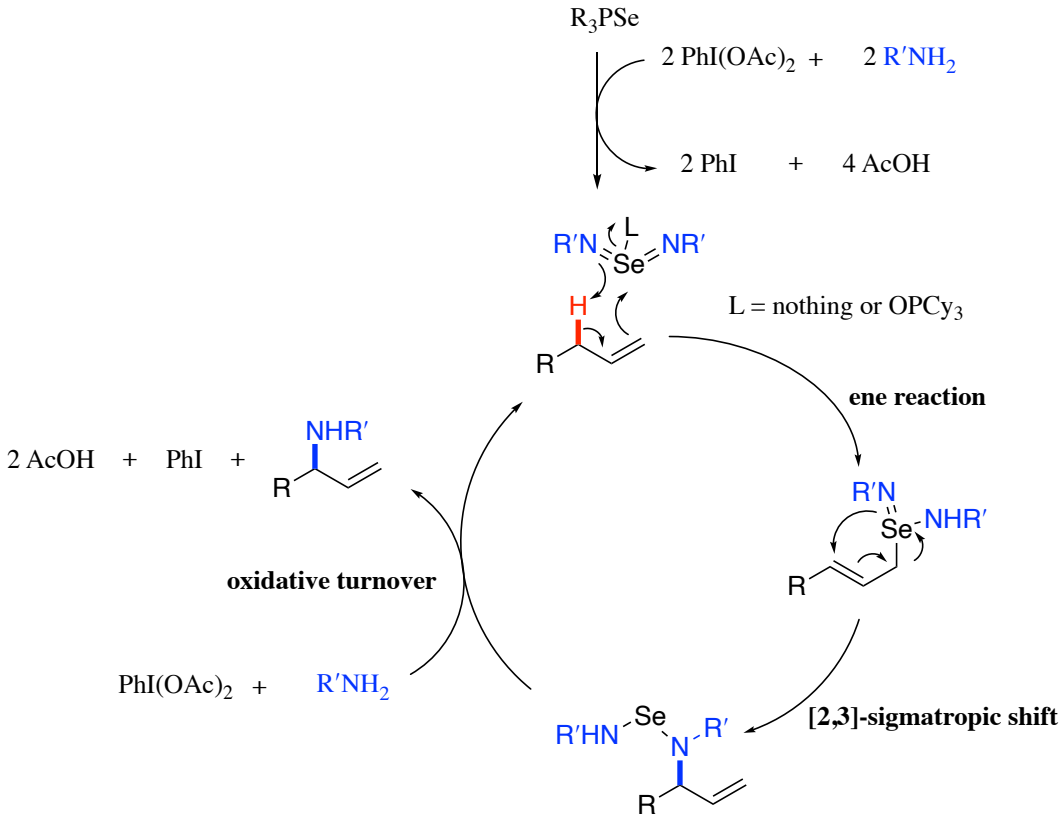

Figure 2.2. Proposed Reaction Mechanism of Allylic Amination

While important contributions, fundamental features of the ene transition state are still unknown and there are many questions left unanswered (Figure 2.3).

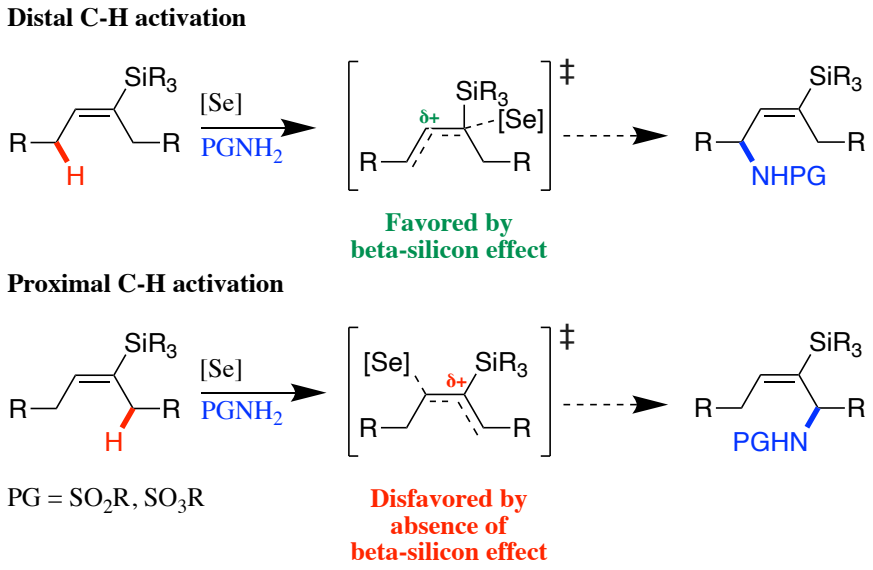

Figure 2.3. Hypothesis for Asynchronous Ene Reaction and Implications for Regioselectivity

For one, we did not know if the ene reaction exhibited asynchronous character. An asynchronous transition state is when bond rupture or formation does not progress to the same extent. Notably, an asynchronous ene reaction is a phenomenon commonly observed when polar enophiles are employed,[4,5] where breaking of the allylic C-H bond is often delayed and formation of the σ Se-C bond is faster. We believed an asynchronous ene reaction could discriminate between multiple allylic C-H bonds in vinylsilanes. The distal site could be favored because partial positive charge is better stabilized through a hyperconjugative event involving the σ Si-C bond, in a manner like the β-silicon effect. The [2,3]-sigmatropic rearrangement step of our chemistry is also understudied, with only one report describing the corresponding transition state on allylic aryl-selenimides.[6] In that study, Bayse only evaluated the preference of endo or exo orientations in the transition state.

By determining the DFT reaction coordinate for amination of vinylsilanes, we could attempt to answer fundamental questions about our chemistry. We would evaluate the characteristics of the ene transition state to assess the preference for distal C-H amination. In addition, our computational study could help us understand the implications of switching the nucleophile from 4-nitrobenzenesulfonamide to trifluoroethyl sulfamate. We previously observed that using trifluoroethyl sulfamate led to formation of a minor amount of the proximal amination product. Our group would assess the magnitude of activation barriers, charge build-up, and bond distances in the ene transition states to answer these important questions.

Section 2: RESULTS AND DISCUSSION

2.1.1 *DFT Reaction Coordinate for Methanesulfonamide Diimide*

DFT calculations were completed using the Gaussian-16 software package to elucidate species in the reaction coordinate.[7-9] Structures were optimized at wB97-XD/6-311++G(d,p) with the polarization continuum model with CH_2Cl_2. Frequency calculations were performed on all structures and enthalpies and free energies were calculated using the harmonic approximation at standard state (1 M concentration). The free energies of activation were adjusted and recorded for 0.04 M concentration to reflect the experimental conditions. Compound **1** (Figure 2.4, green box)

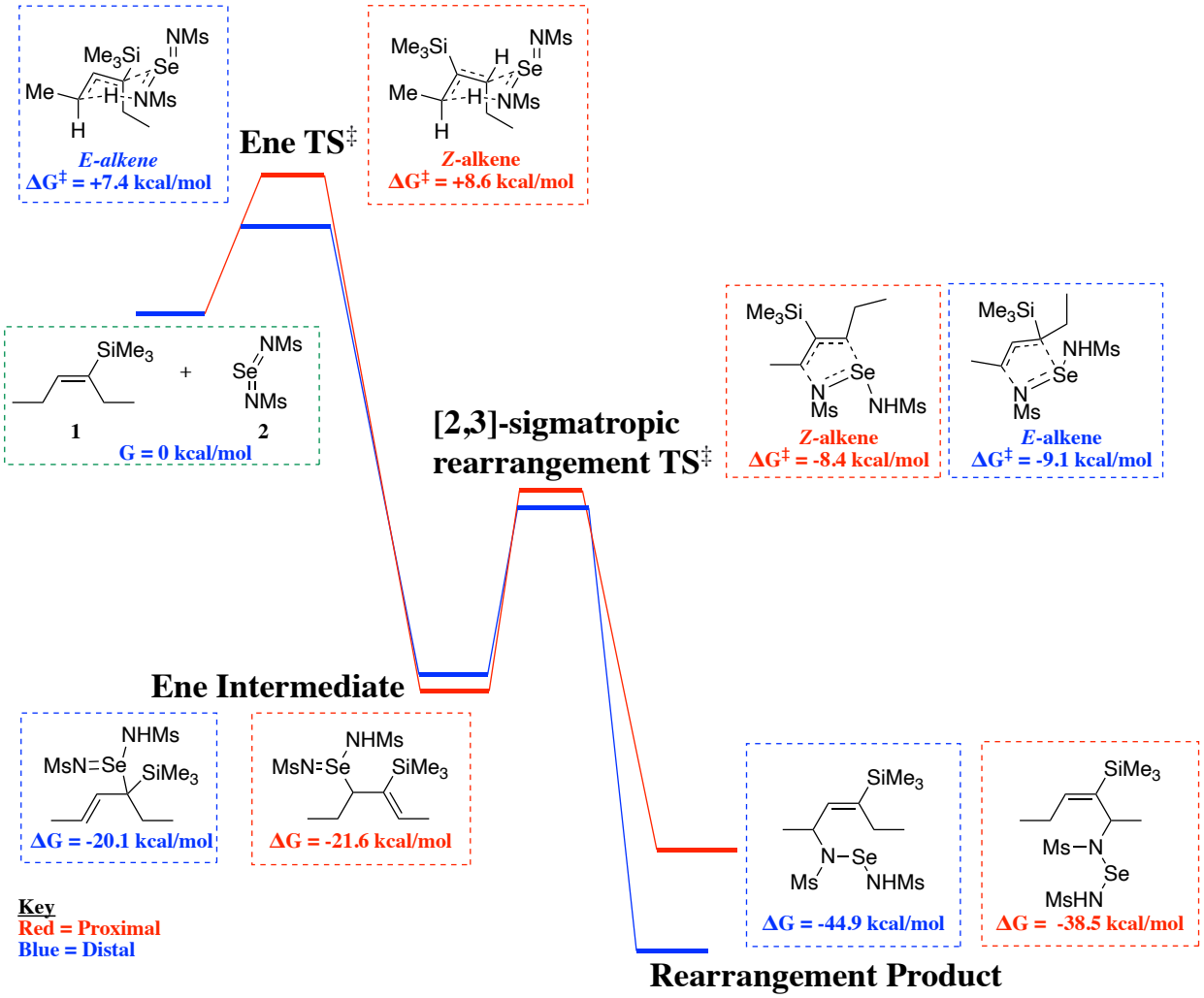

Figure 2.4. DFT Reaction Coordiante for Allylic C-H Amination Between Vinylsilanes and Methanesulfonamide

served as the model vinylsilane reactant, since the substrate scope typically employed silanes with alkyl groups. Selenium diimide **2** is derived from methanesulfonamide and modeled the effect of nosyl amide in our reaction.

This computational study exhibits for the first time the DFT reaction coordinate concerning allylic C-H amination on a vinylsilane substrate. Lowest energy transition states for the ene and rearrangement steps are presented and the reaction pathway for proximal amination is represented by red, whereas the path for distal amination is conveyed in blue. In general, we observe a close race between the two reaction pathways. Our computational work showed that the endo approach was always a lower energy approach for the diimide in the transition state of the ene reaction, generally favored by ~5 kcal/mol. The activation barrier for the distal ene reaction was favored over the proximal case by 1.2 kcal/mol. This difference in free energy was consistent with our experimental findings, where nosyl amide gave exclusively the distal amination product. Short Se-C distances (making up the new σ bond between the enophile and alkene) were observed in both transition states (2.1-2.2 Å), which is consistent with the trends observed in other asynchronous ene reactions (Figure 2.5).[4,5] Whereby Fernández showed that the new σ bond ranged in length from 1.9-2.1 Å.

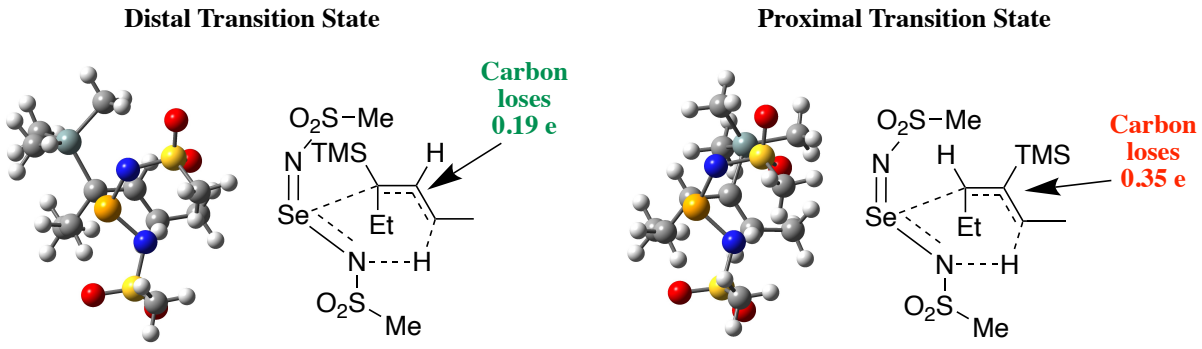

Figure 2.5. Ene Transition States for Distal (Left) and Proximal (Right) with Methanesulfonamide Diimide

Selenium (represented by orange) must attack the vinyl carbon α to the silane to abstract the distal C-H bond. In contrast, selenium attacks the vinyl carbon β to the silane to activate the proximal C-H bond. It was informative to look at the charge build-up in the transition state at the vinyl carbon that's not bound to selenium. To do this, we calculated the NBO charges for the atoms in the transition state and subtracted that value from the corresponding NBO charges in the alkene ground state. Interestingly, the distal case exhibits approximately 50% more electron density at the vinyl carbon in comparison to the proximal case. The greater positive charge build-up in the proximal case is likely destabilizing. We also completed a second order perturbation theory analysis (of the Fock matrix in NBO basis set) for the ene transition states, which helps identify possible hyperconjugation events occurring. A closer look at the distal case reveals an estimated 5.3 kcal/mol hyperconjugation event occurring between σ C-Si into an empty orbital on the adjacent vinyl carbon. This interaction could potentially account for less positive charge build-up in the distal transition state, although other electronic events cannot be excluded at this time.

2.2.2 *Ene Transition States for Methyl Sulfamate Diimide*

Calculations of the ene transition state between the vinylsilane and methoxysulfonyl sulfamate selenium diimide were conducted next. The sulfamate diimide is a model for the trifluoroethanol sulfonamide that was discussed previously, which led to formation of minor quantities of the proximal amination product. We observed a free energy difference (2.6 kcal/mol) between distal and proximal amination, such that the distal case was also favored (Figure 2.6).

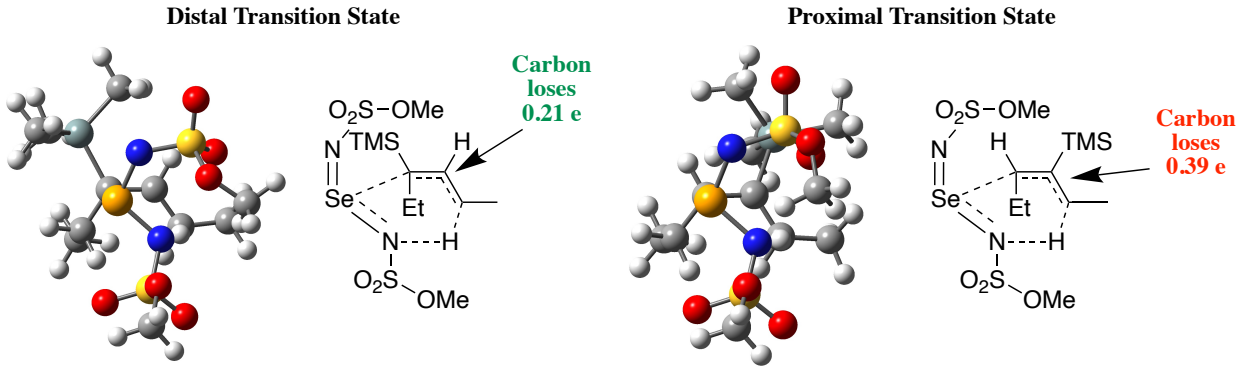

	Nucleophile	Barrier(kcal/mol)	Se-C (Å)	Charge Development at C (e)
Distal	$CH_3OSO_2NH_2$	1.2	2.23	0.21
Proximal	$CH_3OSO_2NH_2$	3.8	2.10	0.39
Distal	$CH_3SO_2NH_2$	7.4	2.26	0.19
Proximal	$CH_3SO_2NH_2$	8.6	2.13	0.35

Figure 2.6. Ene Transition States for Distal (Left) and Proximal (Right) with Methyl Sulfamate Diimide

We observe Se-C distances that were 0.03 Å shorter in these transition states compared to the methanesulfonamide cases, suggesting that the ene transition states here better resemble the ene intermediate. Notably, the activation barriers for the ene reaction using the sulfamate selenium diimide (~4 kcal/mol) were substantially lower in magnitude compared to the methanesulfonamide diimide explored earlier (~8 kcal/mol). The poor regioselectivity for the sulfamate case could be due to the ene reactions being so fast (low ene activation barrier) and the product formed is thus a consequence of diffusion control.

2.2.3 *Vinylsilane vs. Aliphatic Alkene Ene Transition States*

Our group was motivated to gain a greater understanding about how vinylsilanes affect the ene reaction, especially the regioselectivity. To do this, we evaluated the ene transition states of the compounds *Z*-hexene and 3-methyl-3-hexene (Table. 2.1).

Table 2.1. Comparison of Vinylsilane, *Z*-Hexene, and 3-Methyl-3-Hexene Transition States

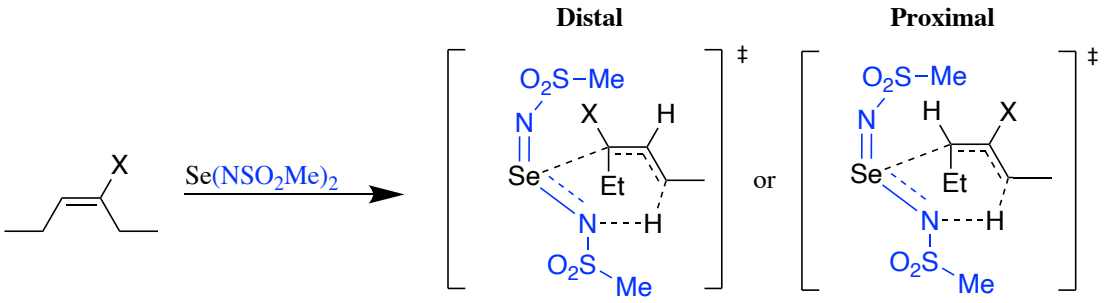

Entry	X	ΔCharge[a] (e)	ΔΔG‡[b] (kcal/mol)
1	H	0.00	0.0
2	Me	-0.05	2.9
3	$SiMe_3$	-0.16	-1.2

[a]ΔCharge is the difference between distal and proximal values for the charge development (charge of transition state minus the ground state) at the vinyl carbon not bound to selenium.
[b]Distal minus proximal transition states values.

Only the syn-anti conformation of the diimide was used for these calculations. The symmetric *Z*-hexene shows identical activation barriers for activating the proximal and distal C-H bonds. Once we substitute the alkene with an atom group other than hydrogen, significant changes occur in the ene transition states. For example, the aliphatic alkene now exhibits a reduced activation barrier for abstracting the proximal C-H bond. This calculation is consistent with our group's previous experimental results on terpenes. The vinylsilane substrate led to the opposite regioselectivity, whereby distal amination was favored. The vinylsilane case also features the greatest amount of charge difference between the two regiodivergent paths. This enhanced charge difference could help support the hypothesis that silane exhibits a large electronic effect on the ene transition state.

We questioned why the proximal ene transition state exhibited enhanced positive charge build-up when X was a silane. To answer this question, we evaluated how the conformation of the

diimide affected the proximal ene transition state energy for 3 types of alkene substrates (Table 2.2).

Table 2.2. Comparison of Diimide Conformations in Proximal Ene Transition States for Vinylsilane, *Z*-Hexene, and 3-Methyl-3-Hexene

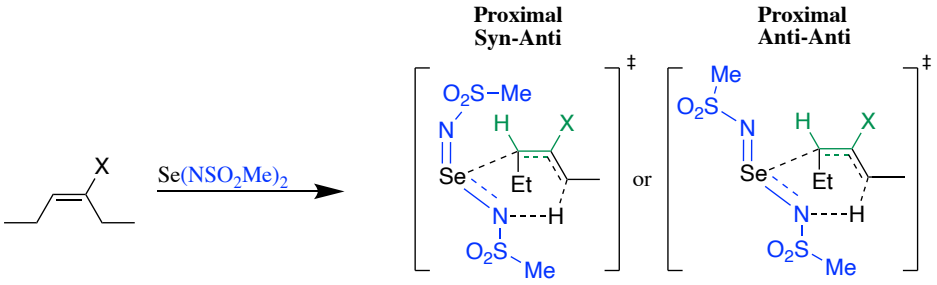

X	ΔCharge[a] Syn-Anti (e)	Dihedral[b] Syn-Anti (°)	ΔSe-C_{mid}[c] (Å)	ΔΔG‡[d] (kcal/mol)
H	0.26	17.6	-0.04	-1.4
Me	0.30	8.7	-0.02	1.3
$SiMe_3$	0.35	-1.6	-0.09	-0.6

[a]ΔCharge is the charge at the vinyl carbon not bound to selenium in ene transitition state minus the alkene ground state. [b]Dihedral angle shown in green. [c]ΔSe-C_{mid} distances involves syn-anti value minus anti-anti. C_{mid} is the carbon alpha to the X group. [d]Proximal ene barriers for the syn-anti case minus the anti-anti case.

The symmetric alkene exhibited a lower ene barrier with the syn-anti conformation of the diimide, where it was favored by 1.4 kcal/mol over the anti-anti diimide. This observation confirmed that the syn-anti diimide leads to the lowest energy ene reaction. However, the syn-anti diimide would cause steric strain between the diimide and X group when X is large, like a silane group. To avoid this scenario, the ene transition state underwent a distortion to minimize this steric strain. The silane group is pushed far back from the face containing the incoming diimide (-1.6 º dihedral in alkene, shown in green). By doing so, the vinyl carbons are pushed forward, and this leads to a shorter Se-C distance and thus more carbocation character in the transition state. We completed a distortion/interaction analysis on the proximal ene transition states in Table 2.2 too. Notably, the syn-anti transition states for the vinylsilane exhibited a distortion in the vinylsilane fragment that was 14.0 kcal/mol greater in energy than when the anti-anti diimide was employed. Whereas the

diimide fragment only experienced minimal distortion, as the syn-anti distortion is 1.1 kcal/mol greater than in the transition state for the anti-anti diimide. Thus, there appears to be a trade-off between steric and electronic effects in the proximal ene transition state. Interestingly, the TMS group can do this distortion with only a minor energy cost.

Section 3: CONCLUSION

For the first time, the reaction coordinate involving allylic C-H amination on a vinylsilane was presented. We observed a possible hyperconjugation event between the σ C-Si into an empty orbital on the adjacent vinyl carbon in the distal ene transition state. This electronic event could play a role in the regioselectivity for distal amination in vinylsilanes. The ene transition states for amination on vinylsilanes were also calculated for a sulfamate diimide to model the effect of trifluoroethanol sulfonamide on the reaction. In this case, the sulfamate diimide led to a significant decrease in the ene activation barrier and a transition state that shared more features with the ene intermediate. We proposed that the poorer regioselectivity in amination using the sulfamate diimide could be related to the fact that the ene activation barrier for each regiodivergent path was very accessible energetically. Whereby the low activation barriers of the ene resulted in diffusion being in control of the regiochemical control. In addition, we compared the ene transition states of a vinylsilane to the ones of *Z*-hexene and 3-methyl-3-hexene. Our results showed that the vinylsilane transition state features the greatest change in charge at the vinyl carbon not bound to selenium. This observation helps support the hypothesis that silane exhibits a greater electronic influence on the ene transition state, leading to a remarkable switch in regioselective amination in comparison to aliphatic alkenes. Analysis of the proximal ene transition states helped identify a

distortion occurring when the syn-anti diimide was employed. The enhanced carbocation character in the proximal transition state can be attributed to minimizing steric strain between the diimide and silane. Overall, the silane provides a small amount of stabilization for distal amination via a β-silicon effect, but almost no stabilization in proximal amination.

Section 4: EXPERIMENTAL

2.4.1 Gene*ral Procedures and Methods*

DFT calculations were performed using the Gaussian-16 software package. Structures were optimized at the wB97-XD/6-311++G(d,p) level of theory, using the PCM model with CH_2Cl_2 as solvent. Frequency calculations were performed on all structures and enthalpies and free energies were calculated using the harmonic approximation at standard state (1 M concentration). Free energies of activation have been adjusted and recorded for 0.04 M concentration to better reflect the experimental conditions. All structures had zero negative frequencies, and the transition state had one negative frequency whose motions corresponded to the expected reaction coordinate.

2.4.2 *Transition States, Reactants, Products, and Intermediates*

Gaussian files are in Michael Group OneDrive/Berman/Thesis Calculation Files/Silane Project. Table 2.3 conveys details of each transition states and the name of the corresponding Gaussian file for reactions of the vinylsilanes.

Table 2.3. Filenames for Transition States Involving Vinylsilanes

Diimide	Reaction & Diimide Conformation	E/Z	Exo/Endo	C-H	Filename (.log ending)
Se(NSO_2Me)	Ene, syn-anti	E	Endo	Distal	distaltmsfromprox382022nbo
Se(NSO_2Me)	Ene, anti-anti	E	Exo	Distal	Ene_dist_nbo_3242021
Se(NSO_2Me)	Ene, anti-anti	Z	Exo	Distal	ene_distz_qst3_3282021
Se(NSO_2Me)	Ene, syn-anti	Z	Endo	Distal	distzoppeneqst24182021
Se(NSO_2Me)	Ene, syn-anti	Z	Endo	Proximal	proxoppsynantivdw8122021_nbo8132021
Se(NSO_2Me)	Ene, anti-anti	Z	Endo	Proximal	proxtmsaa4222022bnbo
Se(NSO_2Me)	Ene, anti-anti	Z	Exo	Proximal	Ene_prox_nbo_3242021
Se(NSO_2Me)	Ene, anti-anti	E	Exo	Proximal	tmszeneproxqst2432021
Se(NSO_2Me)	Ene, syn-anti	E	Endo	Proximal	proxtmsesulfonamide3192022
Se(NSO_3Me)	Ene, syn-anti	E	Endo	Distal	distalsulfamateltmsfromprox3162022nbo
Se(NSO_3Me)	Ene, syn-anti	Z	Endo	Proximal	proxoppsynantiomeberny8172021_nbo8172021
Se(NSO_2Me)	Rearrangement, syn-anti	N/A	Endo	Distal	srdistoppqst3482021
Se(NSO_2Me)	Rearrangement, syn-anti	N/A	Exo	Distal	srdistqst3_422021
Se(NSO_2Me)	Rearrangement, syn-anti	N/A	Endo	Proximal	SigmaRear_prox_qst2_3132021
Se(NSO_2Me)	Rearrangement, syn-anti	N/A	Exo	Proximal	srproxoppqst3472021

Table 2.4 conveys details of the ene transition states and the name of the corresponding Gaussian file for reactions of *Z*-hexene and 3-methyl-3-hexene.

Table 2.4. Filenames for Ene Transition States of *Z*-Hexene and 3-Methyl-3-Hexene

Substrate	C-H Activated	Diimide Conformation	Filename (.log ending)
cis-hexene	Distal/Proximal	Syn-anti	proxcishexenesulfonamide372022nbo

cis-hexene	Distal/Proximal	Anti-anti	proxcishexenesantianti3302022nbo
3-methyl-3-hexene	Distal	Syn-anti	distal3methylhexenefromprox382022nbo
3-methyl-3-hexene	Proximal	Syn-anti	proxch3sulfonamide322022nbo
3-methyl-3-hexene	Proximal	Anti-anti	proxantianti3302022_3methyl4202022nbo

Table 2.5 conveys details of the reactants, intermediates, or products and the name of the corresponding Gaussian files.

Table 2.5. Filenames for Reactants, Intermediates, and Products

Compound	**Filename (.log ending)**
[(*1E*)-1-Ethyl-1-buten-1-yl]trimethylsilane	TMS_SM_opt_freq
Se(NSO_2Me) – syn/anti	MethaneSulfonate_diimide_opt_freq
Se(NSO_2Me) – anti/anti	diimideantiantiopt612021
Se(NSO_3Me) – syn/anti	Sulfamate_syn_optfreq_3232021
Se(NSO_3Me) – anti/anti	Sulfamate_anti_optfreq_3232021
Proximal ene intermediate (Z alkene)	TMS_Ene_Prox_conf_DFT_NBO_opt_freq
Distal ene intermediate (E alkene)	TMS_Ene_Dist_conf_DFT_NBO_opt_freq
Proximal rearrangement intermediate	TMS_SigmaRear_Proximal_opt_freq
Distal rearrangement intermediate	JLB01007
Cis-hexene	cishexenesm372022
3-methyl-3-hexene	3methylhexenenbo332022

The Distortion/Interaction Analysis excel sheet is in Michael Group OneDrive/Berman/Thesis Calculation Files/Silane Project/Distortion Interaction Files/Distoriton Interaction Sheet.xlsx. The filenames for each Gaussian fragment match those in the tables beforehand, but the fragment is indicated by the suffix of the file (i.e. alkene or diimide).

REFERENCES FOR CHAPTER 2

[1] Precedence for the ene step. (a) Sharpless, K. B.; Jensen, H. P.; Vasella, A.; Arigoni, D. *J. Am. Chem. Soc.* **1973,** *95,* 7917-7919. (b) Sharpless, K. B.; Lauer, R. F. *J. Am. Chem. Soc.* **1972,** *94,* 7154-7155. (c) Stephenson, L. M.; Speth, D. R. *J. Org. Chem.* **1979,** *44,* 4683-4689.

[2] Sharpless, K. B.; Lauer, R. F. *J. Am. Chem. Soc.* **1972,** *94,* 7154-7155.

[3] Teh, W. P.; Obenschain, D. C.; Black, B. M.; Michael, F. E. *J. Am. Chem. Soc.* **2020,** *142,* 16716-16722.

[4] Pederes, G. D.; Jorgensen, W. L. *J. Org. Chem.* **1992,** *57,* 1904-1916.

[5] Fernández, I.; Bickelhaupt, F. M. *J. Comput. Chem.* **2012,** *33,* 509-516.

[6] Antony, S.; Bayse. C. A. *Molecules,* **2009,** *14,* 3229-3236.

[7] Gaussian 16, Revision B.01, Frisch, M. J.; Trucks, G. W.; Schlegel, H. B.; Scuseria, G. E.; Robb, M. A.; Cheeseman, J. R.; Scalmani, G.; Barone, V.; Petersson, G. A.; Nakatsuji, H.; Li, X.; Caricato, M.; Marenich, A. V.; Bloino, J.; Janesko, B. G.; Gomperts, R.; Mennucci, B.; Hratchian, H. P.; Ortiz, J. V.; Izmaylov, A. F.; Sonnenberg, J. L.; Williams-Young, D.; Ding, F.; Lipparini, F.; Egidi, F.; Goings, J.; Peng, B.; Petrone, A.; Henderson, T.; Ranasinghe, D.; Zakrzewski, V. G.; Gao, J.; Rega, N.; Zheng, G.; Liang, W.; Hada, M.; Ehara, M.; Toyota, K.; Fukuda, R.; Hasegawa, J.; Ishida, M.; Nakajima, T.; Honda, Y.; Kitao, O.; Nakai, H.; Vreven, T.; Throssell, K.; Montgomery, J. A., Jr.; Peralta, J. E.; Ogliaro, F.; Bearpark, M. J.; Heyd, J. J.; Brothers, E. N.; Kudin, K. N.; Staroverov, V. N.; Keith, T. A.; Kobayashi, R.; Normand, J.; Raghavachari, K.; Rendell, A. P.; Burant, J. C.; Iyengar, S. S.; Tomasi, J.; Cossi, M.; Millam, J. M.; Klene, M.; Adamo, C.; Cammi, R.; Ochterski, J. W.; Martin, R. L.;

Morokuma, K.; Farkas, O.; Foresman, J. B.; Fox, D. J. Gaussian, Inc., Wallingford CT, 2016.

[8] NBO Version 3.1, Glendening, E. D.; Reed, A. E.; Carpenter, J. E.; Weinhold, F.

[9] Avogadro: an open-source molecular builder and vis-ualization tool. Version 1.2.0. http://avogadro.cc/. Marcus D Hanwell, Donald E Curtis, David C Lonie, Tim Vandermeersch, Eva Zurek and Geoffrey R Hutchison; "Avogadro: An advanced semantic chemical editor, visualiza-tion, and analysis platform" Journal of Cheminformatics 2012, 4:17.

Chapter 3. DIASTEREOSELECTIVE C-H AMINATION

Section 1: INTRODUCTION

Encountered in both pharmaceuticals and asymmetric catalysts, vicinal amino alcohols are an important synthetic target.[1] Among these compounds are 1,4- and 1,2-aminoalcohols, whereby the latter can be made via a plethora of functional group conversions.[2] Direct C-H functionalization methods to make these molecules are highly desirable because they are atom-economical.[3] There are methods to synthesize 1,2-aminoalcohols via C-H amination and they can involve radical chemistry[4] or transition-metal catalysis.[5] However, diastereoselective versions of these reactions are so far limited to intramolecular transformations[6] and they do no generate a desirable quaternary stereocenter (Figure 3.1).

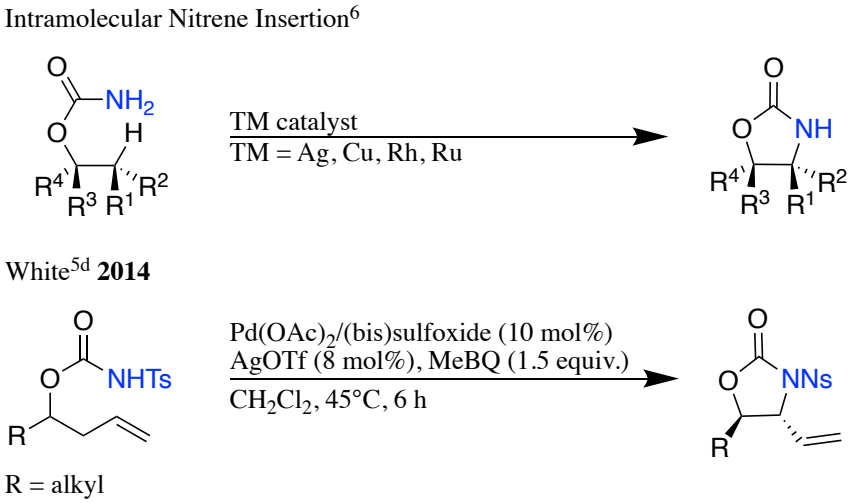

Figure 3.1. Intramolecular C-H Amination

In addition, there appear to be no reports disclosing a diastereoselective synthesis of 1,4-aminoalcohols.

Our group addressed these outstanding challenges by adapting our selenium-catalyzed allylic C-H amination chemistry to make 1,2- and 1,4-aminoalcohols.[7] Experimental work in this area was accomplished by Dr. Tianyi Zheng in our research group. Fortunately, diastereoselective formation of *anti*-1,2-amino protected alcohols occurred (Figure 3.2, top).

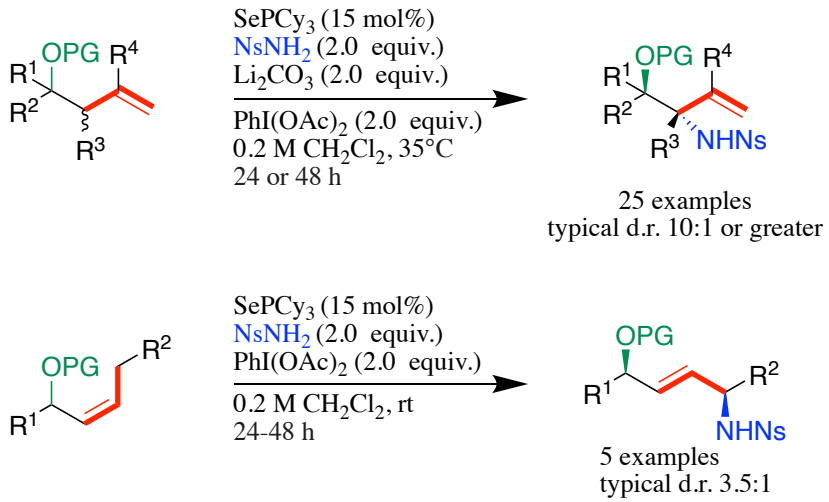

Figure 3.2. Synthesis of *Anti*-1,2-Products (Top) and *Syn*-1,4-Products (Bottom)

However, we questioned why diastereoselective amination occurred. When a carbon-bound homoallylic ester was subjected to the reaction, poor diastereoselectivity was observed. This experiment confirmed the importance of the oxygen-bound homoallylic ester to induce stereoinduction, but it was unclear what the mechanism involved. Another diastereoselective outcome worth investigating was the generation of *syn*-1,4-products from *Z*-alkenes (Figure 3.2, bottom). We hypothesized that the diastereoselective step was linked to the steric demands in the ene reaction. The *Z*-geometry of the substrates likely decreased conformational flexibility in the ene transition state, such that building $A_{1,3}$ strain could play a role in deciding the diastereoselective outcome. Using computational chemistry, we aimed to study the C-H allylic amination mechanism to elucidate reasons for diastereoselectivity in these cases. This computational study was further

required to identify the predominant diastereomer formed in our reaction to make 1,4-products, since our group was unable to identify it experimentally.

Section 2: RESULTS AND DISCUSSION

3.2.1 *Formation of Anti-1,2-Products – Homoallyl Fluoride Model*

We hypothesized that the [2,3]-sigmatropic rearrangement step was the stereodetermining step in making our 1,2-amino protected alcohols (Figure 3.3).

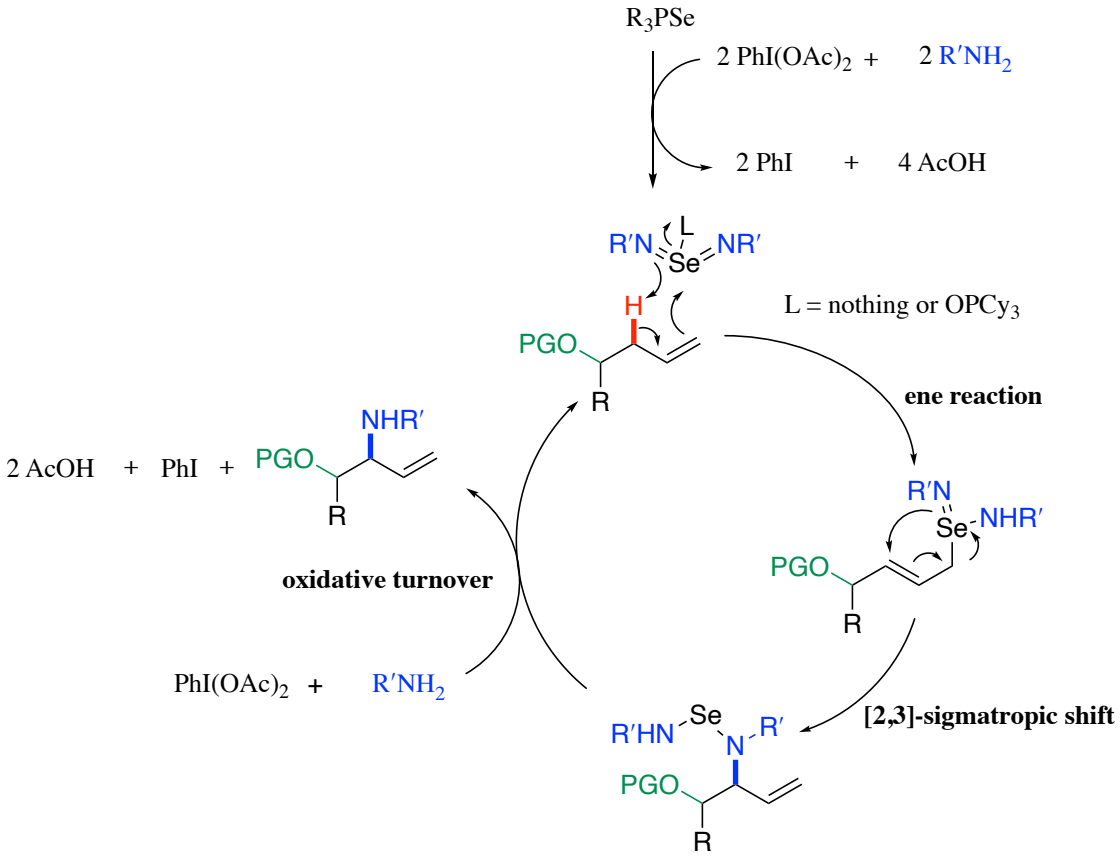

Figure 3.3. Proposed Mechanism of Allylic C-H Amination to *Anti*-1,2-Products

The allylic stereocenter is first destroyed in the starting material during the ene reaction, then reformed during the rearrangement step. Thus, the rearrangement occurs near the protected alcohol and stereoinduction could occur via an electronic or steric effect. To test this idea, we planned to study how the conformation of the protected alcohol affected the transition state energy of the rearrangement and thus the diastereoselectivity of the transformation.

We began our study by investigating homoallyl fluorides in the [2,3]-sigmatropic rearrangement step. We chose homoallyl fluorides as model substrates because they exhibit a polar C-F bond, thus modeling the C-O bond of homoallyl acetates that were used in our reaction. We hypothesized that there would be a correlation involving the energy of the ene intermediate and the transition state energy of the rearrangement. In the scenario that there was no such correlation, we planned to elucidate a stereoelectronic effect that may be responsible for the discrepancy. Whereby the diastereochemical outcome is a consequence of a required spatial arrangement of molecular orbitals in the rearrangement transition state, perhaps stabilize the transition state through an electronic effect. We first evaluated the stability of homoallyl fluorides (Figure 3.4) in the simplified ene intermediates and the transition state energies for the [2,3]-sigmatropic

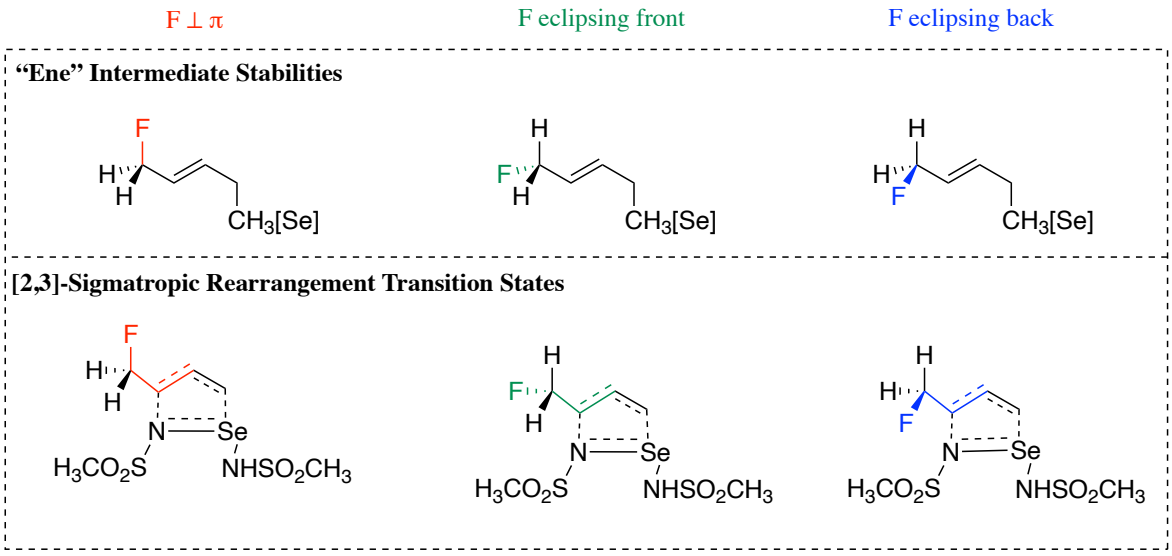

Figure 3.4. Simplified Ene Intermediates and [2,3]-Sigmatropic Rearrangement Transition States for Homoallyl Fluorides

rearrangement. For the ene compounds, methyl represented selenium to simplify our calculations. Three conformations of the C-F bond were explored, and these included the scenarios of fluorine being perpendicular to the π system, eclipsing from the front (inside), or eclipsing from the back (outside) of the alkene.

To our surprise, the lowest energy rearrangement transition state did not involve the most stable ene intermediate, this was the case of fluorine occupying an inside position. A closer look at the rearrangement transition states led to an interesting observation. A very strong correlation (Figure 3.5) can be observed between activation barrier and electron donation into π^*

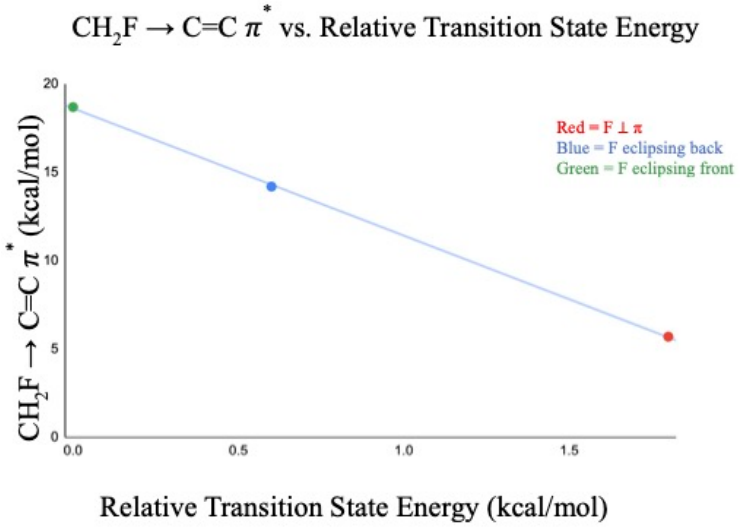

Figure 3.5. Electron Donation into π System vs. Relative Transition State Energy of Homoallyl Fluorides

during the [2,3]-sigmatropic rearrangement transition state. The x-axis contains the relative energies of the transition states for each fluorine conformation. The y-axis is the sum of the C-F and C-H σ bond donations into π^* star in the corresponding transition states, which was estimated by a second order perturbation theory analysis (of the Fock matrix in NBO basis set). The inside position of fluorine exhibited the lowest activation barrier and the greatest magnitude of electron

donation into the π system. This feature contributed to the enhanced charge transfer between the substrate and the selenium imide fragment, making the transition state looser (Figure 3.6).

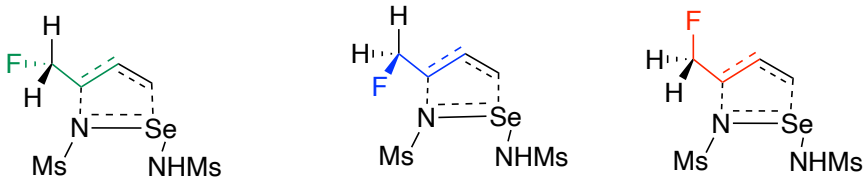

transition state	inside	outside	anti
θ(°)	-89	+64	+163
charge transfer from substrate to Se=N (e)	0.42	0.35	0.33
relative energy (kcal/mol)	0	0.6	1.8
C-Se bond length (Å)	2.68	2.60	2.62
C-N bond length (Å)	2.30	2.30	2.25
sum of bond lengths (Å)	4.98	4.90	4.87

Figure 3.6. Comparison of [2,3]-Sigmatropic Rearrangement Transition States for Homoallyl Fluorides

Notably, the same analysis was done with homoallyl acetates (Experimental, Table 3.2) and the results are consistent with the fluoride study.

The phenomenon we observed is a type of inside alkoxy effect[8-10] (Figure 3.7), such that

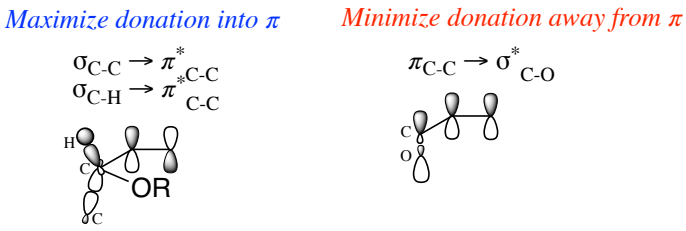

Figure 3.7. Inside Alkoxy Effect Orbital Pictures

the polar C-X bond prefers an inside position in relation to the alkene in the transition state. Houk previously elucidated this phenomenon in [3+2] cycloadditions and asserted that the inside conformation was preferred for mainly electronic reasons, whereby the inside C-O bond enhanced C-C and C-H σ bond donation into the π^*, which stabilized the electrophilic π system in the

transition state. Notably, the inside conformation also minimized the destabilizing interaction from overlap between the C-O σ^* and π system. Our computational study on homoallyl fluorides thus suggests that the polar C-F shares the conformational preference for an inside position for similar reasons. Overall, this calculation represents the first case of an inside alkoxy effect in a [2,3]-sigmatropic rearrangement.

3.2.2 *Formation of Anti-1,2-Products – Homoallyl Acetate Model*

A computational study was next extended to homoallyl acetates because they more accurately model the substrates used in our reaction. We determined the [2,3]-sigmatropic rearrangement transition states that led to the *syn*- or *anti*-products (Figure 3.8).

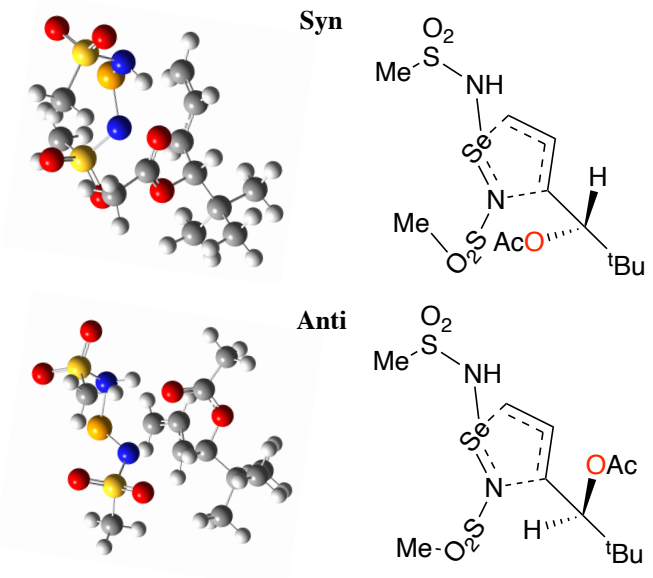

transition state	Anti	Syn	Δ (Anti-Syn)
charge transfer from substrate to Se=N (e)	0.288	0.248	0.04
relative energy (kcal/mol)	0	+2.6	-2.6
C-Se bond length (Å)	2.57	2.53	0.04
C-N bond length (Å)	2.18	2.14	0.04

Figure 3.8. [2,3]-Sigmatropic Rearrangement Transition States for Homoallyl Acetates

There was a 2.6 kcal/mol difference between the transition states leading to the *syn* or *anti* diastereomers. The *anti*-isomer with the inside acetyl group was favored computationally, agreeing with the experimental result that showed exclusive formation of the *anti*-product. Closer analysis also showed that the *anti*-transition state features enhanced charge transfer between the substrate and imide fragment as well as a looser transition state. These observations are consistent with the inside alkoxy effect and can justify the diastereoselectivity for the *anti*-product.

3.2.3 *Formation of Syn-1,4-Products*

Further computational work was done to understand the diastereoselective preference to form *syn*-1,4-amino protected alcohols in our reaction. We utilized a model substrate containing an acetyl group at an allylic position that is at the site opposite to where amination occurred. Ene transition states featuring an endo approach were calculated and we studied how conformations at the allylic site affected the activation barrier (Figure 3.9).

Stereochemistry of final amination product	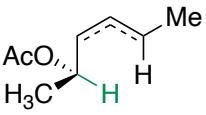	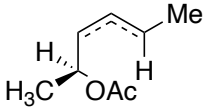	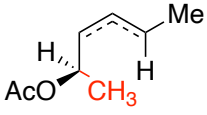
Syn 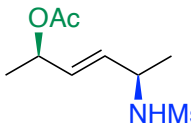	0.0	+2.8	+5.3
Anti 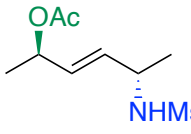	+0.4	+2.0	+4.2

Figure 3.9. Relative Energy (kcal/mol) of Ene Transition States for 1,4-Aminoalcohols

We determined that the lowest activation barrier was associated with the transition state that minimized $A_{1,3}$ strain, which coincides with the hydrogen atom eclipsing with the alkene in the syn-transition state. When comparing the *anti* and *syn* versions for this case, the *syn* diastereomeric transition state was lower in energy and favored by 0.4 kcal/mol over the *anti*-diastereomeric transition state (Figure 3.10).

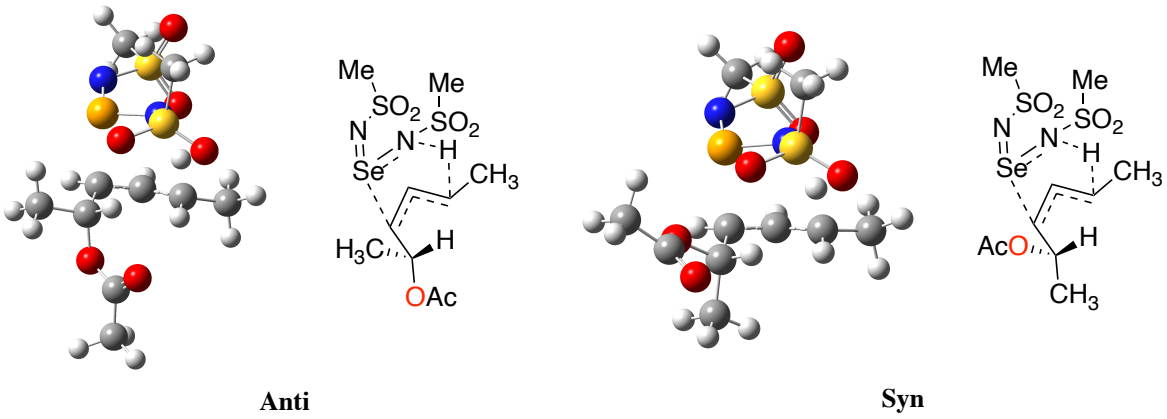

Figure 3.10. Lowest Energy Ene Transition States for 1,4-Aminoalcohols

Our group was unable to verify the predominant diastereomer experimentally, but the computational result informs us enough to confidently assign the final product as the *syn*-diastereomer. The free energy difference calculated (2:1) equates to a slightly lower diastereomer ratio than is expected based on experiment (3.5:1). The preference to make the *syn*-1,4-aminoalcohol could be related to the reduced steric clashes that occur when the diimide approaches the face containing the acetate. Whereas forming the *anti*-product would require the diimide to attack from the side of the alkene that features the bulkier methyl group.

Section 3: CONCLUSION

In summary, a DFT computational study was completed to better understand the diastereoselective outcomes of our allylic amination reaction. We showed that the inside alkoxy effect was consequential in making *anti*-1,2-aminoalcohols, which to our knowledge is the first time that phenomenon is implicated in a [2,3]-sigmatropic rearrangement. We also evaluated how $A_{1,3}$ strain played an important role in deciding the preference of making *syn*-1,4-aminoalcohols.

Section 4: EXPERIMENTAL

3.4.1 *General Procedures and Methods*

DFT calculations were performed using the Gaussian-16 software package. Structures were optimized at the wB97-XD/6-311++G(d,p) level of theory, using the PCM model with CH_2Cl_2 as solvent. Frequency calculations were performed on all structures and enthalpies and free energies were calculated using the harmonic approximation at standard state (1 M concentration). Free energies of activation have been adjusted and recorded for 0.04 M concentration to better reflect the experimental conditions. All structures had zero negative frequencies, and the transition state had one negative frequency whose motions corresponded to the expected reaction coordinate.

3.4.2 *Transition States and Intermediates*

Gaussian files are in Michael Group OneDrive/Berman/Thesis Calculation Files/Diastereoselective Amination Project. Table 3.1 conveys details of transition states,

intermediates, and the name of the corresponding Gaussian file for reactions of the homoallyl fluorides.

Table 3.1. Filenames for Transition States and Intermediates for Homoallyl Fluorides

Compound	Filename (.log ending)
Simplified ene intermediate - fluoride perpendicular/anti	hfeneantiopt8162021
Simplified ene intermediate - fluoride inside	hfeneeclipfrontredoopt8162021
Simplified ene intermediate - fluoride outside	hfeneeclipbackopt8162021
Transition State for Sigmatropic Rearrangement – fluoride perpendicular/anti	hfantiexoberny8122021_orb8142021
Transition State for Sigmatropic Rearrangement – fluoride inside	hfeclipfrontexoberny8122021_orb8142021
Transition State for Sigmatropic Rearrangement – fluoride inside	hfeclipbackexoberny8122021_orb8142021

Table 3.2 conveys details of transition states, reactants, intermediates, and the name of the corresponding Gaussian file for reactions of the homoallyl acetates.

Table 3.2. Filenames for Transition States, Reactants, and Intermediates for Homoallyl Acetates

Compound	Filename (.log ending)
Simplified ene intermediate – acetate perpendicular/anti	hameantiopt6122021
Simplified ene intermediate – acetate inside	hameeclipfrontredoopt612021
Simplified ene intermediate – acetate outside	hameeclipbackagain672021
Transition State for Sigmatropic Rearrangement – acetate perpendicular/anti	haantieneoptimi552021_nbo7162021
Transition State for Sigmatropic Rearrangement – acetate inside	allylacetateeneeclipfrontop522021_nbo7162021
Transition State for Sigmatropic Rearrangement – acetate inside	allylacetateeclipbackene4262021_nbo7162021

Table 3.3 conveys details of the transition states for the [2,3]-sigmatropic rearrangement and the corresponding Gaussian file for reactions of the homoallyl acetate containing a tert-butyl group γ to the alkene.

Table 3.3. Filenames for Transition States for Homoallyl Acetate with ^{t}Butyl γ to the Alkene

Diastereomer	**Filename (.log ending)**
Anti	tbuantiqst3a8232021_nbo8232021
Syn	tbusynendoqst37282021_nbo7292021

Table 3.4 conveys details of the transition states for the [2,3]-sigmatropic rearrangement and the corresponding Gaussian file for the ene reactions of the *Z*-alkene.

Table 3.4. Filenames for Transition States for *Z*-Alkene in Ene Reaction

Diastereomer	**Atom Group Eclipsed with Alkene**	**Filename (.log ending)**
Anti	H	haazabackberny8262021_nbo8272021
Syn	H	haazabackcdownberny8282021_nbo8282021
Anti	OAc	haazcbackberny8262021_nbo8272021
Syn	OAc	haazqst2a8262021_nbo8262021
Anti	Me	haazcfrontoacbackberny1172021m
Syn	Me	haazcfrontberny1162021m

REFERENCES FOR CHAPTER 3

[1] (a) Lee, H.-S.; Kang, S. H. *Synlett* **2004,** 1673–1685 and references therein. (b) Pu, L; Yu, H.-B. *Chem. Rev.* **2001,** *101,* 757–824. (c) Ager, D. J.; Prakash, I.; Schaad, D. *Chem. Rev.* **1996,** *96,* 835–876.

[2] Traditional methods to make 1,2-amino alcohols can involve epoxides. (a) Kumar, M.; Kureshy, R. I.; Saravanan, S.; Verma, S.; Jakhar, A.; Khan, N. H.; Abdi, S. H. R.; Bajaj, H. C. *Org. Lett.* **2014,** *16,* 2798–2801. (b) Wang, C.; Yamamoto, H. *J. Am. Chem. Soc.* **2014,** *136,* 6888–6891. (c) Schaus, S. E.; Larrow, J. F.; Jacobsen, E. N. *J. Org. Chem.* **1997,** *62*, 4197–4199. (d) Hou, X.-L.; Wu, J.; Dai, L.-X.; Xia, L.-J.; Tang, M.-H. *Tetrahedron Asymmetry* **1998,** *9*, 1747–1752. (e) Bartoli, G.; Bosco, M.; Carlone, A.; Locatelli, M.; Massaccesi, M.; Melchiorre, P.; Sambri, L. *Org. Lett.* **2004,** *6*, 2173–2176. (f) Olofsson, B.; Khamrai, U.; Somfai, P. *Org. Lett.* **2000,** *2*, 4087–4089. Use aziridines (g) Bergmeier, S. C.; Stanchina, D. M. *J. Org. Chem.* **1997,** *62*, 4449–4456. Use enamines and imines (h) Fisher, G. B.; Goralski, C. T.; Nicholson, L. W.; Hasha, D. L.; Zakett, D.; Singaram, B. *J. Org. Chem.* **1995,** *60*, 2026–2034. Use olefins (i) Bodkin, J. A.; McLeod, M. D. *J. Chem. Soc. Perkin 1* **2002,** 2733–2746.

[3] (a) Daview, H. M. L.; Manning, J. R. *Nature* **2008,** *451,* 417–424. (b) Gutekunst, W. R.; Baran, P. S. *Chem. Soc. Rev.* **2011,** *40,* 1976. (c) McMurray, L.; O'Hara, F.; Gaunt, M. J. *Chem. Soc. Rev.* **2011,** *40,* 1885.

[4] (a) Mou, X.-Q.; Chen, X.-Y.; Chen, G.; He, G. Chem. *Commun.* **2018,** *54,* 515–518. (b) Nakafuku, K. M.;, Zhang, Z.; Wappes, E. A.; Stateman, L. M.; Chen, A. D.; D. Nagib, A. *Nat. Chem.* **2020,** *12,* 697–704. (c) Wappes, E. A.; Nakafuku, K. M.; Nagib, D. A. J. *Am. Chem. Soc.* **2017,** *139,* 10204–10207.

[5] Intermolecular transformations (a) Dong, Y.; Chen, J.; Xu, H. *Chem. Commun.* **2018,** *54,* 11096–11099. (b) Dong, Y.; Liu, G. *J. Org. Chem.* **2017,** *82,* 3864–3872. (c) Jin, L.; Zeng, X.; Li, S.; Hong, X.; Qiu, G.; Liu, P. *Chem. Commun.* **2017,** *53,* 3986–3989. Intramolecular transformations (d) Osberger, T. J.; White, M. C. *J. Am. Chem. Soc.* **2014,**

136, 11176–11181. (e) Fraunhoffer, K. J.; White, M. C. *J. Am. Chem. Soc.* **2007,** *129,* 7274–7276. (f) Strambeanu, I. I.; White, M. C. *J. Am. Chem. Soc.* **2013,** *135,* 12032–12037.

[6] There are examples of diastereoselective intramolecular C-H amination reactions involving nitrene insertions. Examples using rhodium (a) Lebel, H.; Huard, K.; Lectard, S. *J. Am. Chem. Soc.* **2005,** *127,* 14198–14199. (b) Lebel, H.; Mamani Laparra, L; Khalifa, M.; Trudel, C.; Audubert, C.; Szponarski, M.; Dicaire Leduc, C.; Azek, E.; Ernzerhof, M. *Org. Biomol. Chem.* **2017,** *15,* 4144–4158. (c) Espino, C. G.; Du Bois, J. *Angew. Chem. Int. Ed.* **2001,** *40,* 598–600. Example using silver (d) Ju, M.; Huang, M.; Vine, L. E.; Dehghany, M.; Robert, J. M.; Schomaker, J. M. *Nat. Catal.* **2019,** *2,* 899–908. Example using ruthenium (e) Milczek, E.; Boudet, N.; Blakey, S. *Angew. Chem. Int. Ed.* **2008,** *47,* 6825–6828. Example using copper (f) Barman, D. N.; Nicholas, K. M.; *Eur. J. Org. Chem.* **2011,** *2011,* 908–911.

[7] Zheng, T.; Berman, J. L.; Michael, F. *Manuscript Submitted.*

[8] Houk, K. N.; Moses, S. R.; Wu, Y.-D. Rondan, N. G.; Jäger, V.; Schohe, R.; Fronczek, F. R. *J. Am. Chem. Soc.* **1984,** *106,* 3880-3882.

[9] Raimondi, L.; Wu, Y.-D.; Brown, F. K.; Houk, K. N. *Tet. Lett.* **1992,** *33,* 4409-4412.

[10] Haller, J.; Strassner, T.; Houk, K. N. *J. Am. Chem. Soc.* **1997,** *119,* 8031-8034.

Chapter 4. IMPLICATIONS OF DIRECTING GROUPS IN ENE OF ALLYLIC C-H AMINATION

Section 1: INTRODUCTION

The utility of our amination method could be increased if it were applicable to substrates containing multiple allylic C-H bonds, such as disubstituted alkenes (Figure 4.1). A challenge with

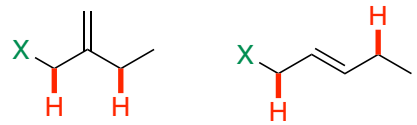

X = SiR_3, BR_2, OR, NR_2, CO_2R, halogen

Figure 4.1. Application of Directing Groups (X) in Allylic C-H Amination of 1,1- and 1,2-Disubstituted Alkenes

this prospect is activating one allylic C-H bond among others that are in very similar chemical environments. We hypothesized that selectivity of allylic C-H bonds could be enhanced if one functional group is remotely located to one allylic site. The ene step is responsible for abstracting the allylic C-H bond and is the product determining step of our amination reaction. The electronic properties of the X group could potentially affect the ene transition state energy and the reaction regioselectivity. Precedence for this remote directing strategy can be found in recent publications. For example, Rovis[1] presented an Ir-catalyzed allylic amination reaction that led to regioselective installation of sulfonamides in unsymmetrically substituted alkenes. Rovis observed that inductively withdrawing groups deactivated the allylic C-H bond nearby and thus promoted amination at the remote site. This reaction was successful on 1,1- and 1,2-disubstituted alkenes, while also using X groups with diverse electronic properties (Figure 4.2). Our group also showed

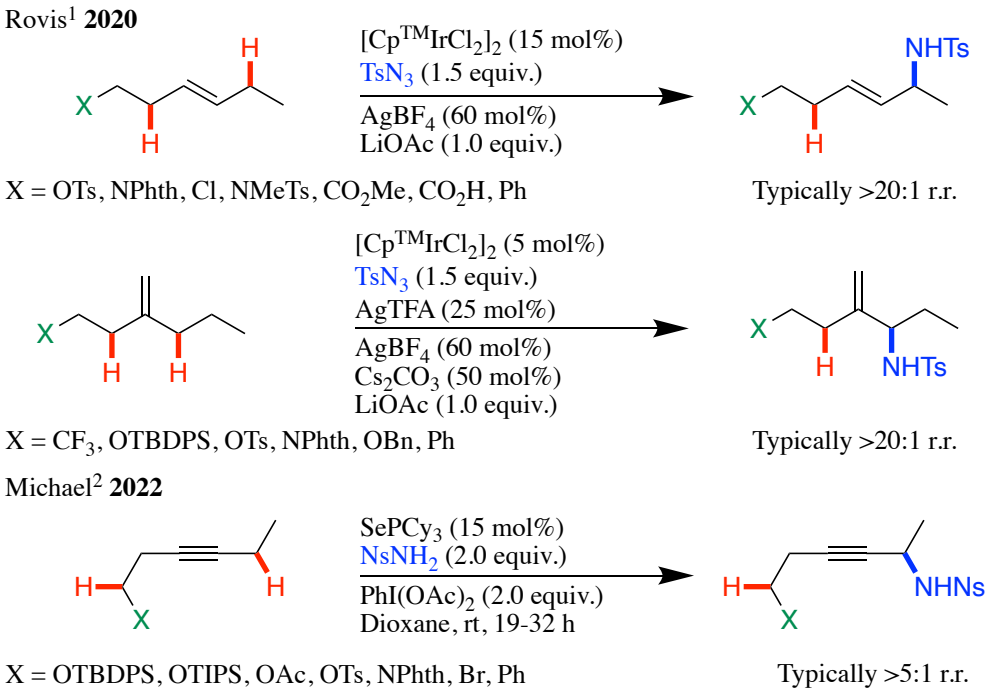

Figure 4.2. Select Examples of Regioselective Amination Through Remote X Groups

that our selenium catalyzed amination reaction was capable of regioselective amination of propargylic protons.[2] We hypothesized that regioselective amination of allylic C-H bonds would be plausible too through remote directing groups. We completed a computational study to elucidate which 1,1- and 1,2- disubstituted alkene substrates would be successful in regioselective amination and created a mathematical model to predict the regioselectivity for any substrate in these classes. Another gap in the knowledge is how electronically diverse alkenes affect the ene reaction, since studies have only been completed on propene.[5] A next step will be to evaluate how X groups at the vinylic position of the alkene affect the ene transition state barrier and determine a mathematical model to predict an ene barrier.

Section 2: RESULTS AND DISCUSSION

Section 4.2.1. *Directing Effects in 1,2-Disubstituted Alkenes*

The ene reaction of 1,2-disubstituted alkenes was first examined by calculating the transition states for amination near X (Figure 4.3).

more concerted

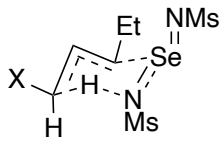

X= EWG

more carbocation character

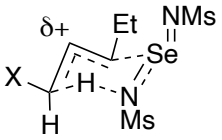

X= EDG

X	N-H (Å)	Allylic C-H (Å)
CH_2F	1.52	1.24
CO_2Me	1.52	1.24
CH_2CF_3	1.53	1.23
CH_2Cl	1.53	1.23
F	1.53	1.23
CH_2OCOMe	1.53	1.23
OCOMe	1.53	1.23
$CH_2NHCOMe$	1.54	1.23
CH_2OMe	1.54	1.23
Et	1.60	1.21
Me	1.61	1.21
OMe	1.62	1.21
Ph	1.64	1.20
CH_2TMS	1.65	1.20

Figure 4.3. Ene Transition State Data for Amination Near X in 1,2-Disubstituted Alkenes

The Se-C distances were nearly constant (~2.1 Å), but the N-H bond distance in the transition state varied according to the X group identity. Electron-withdrawing X groups had shorter N-H distances (~1.5 Å) compared to electron-releasing X groups (~1.6 Å). There was an inverse relationship between N-H and the allylic C-H bond lengths, for example, long N-H bonds were associated with a less broken (shorter) allylic C-H bond. This observation suggests that electron-releasing groups led to an ene transition state with more carbocation character, which could be stabilized inductively by the X group. Conversely, electron-withdrawing groups had a more concerted ene transition state and thus less carbocation character, which would be destabilized

inductively by the X group. These findings help support the influence of these remote X groups in the reactivity of 1,2-disubstituted alkenes and we were motivated to investigate if they can be crucial in achieving regioselective amination.

Towards this goal, we determined the ene reaction energy barrier for amination at each allylic site and calculated $\Delta\Delta G^{\ddagger}$ that describes the difference in those ene activation barriers (Figure 4.4).

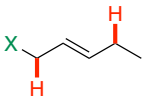

X	$\Delta G^{\ddagger}$ Near (kcal/mol)	$\Delta G^{\ddagger}$ Far (kcal/mol)	$\Delta\Delta G^{\ddagger}$ (kcal/mol)	Exothermicity (kcal/mol)
CH_2TMS	6.8	8.5	-1.6	-1.4
CH_2CF_3	8.7	10.4	-1.6	0.2
CH_2Cl	9.6	10.4	-0.7	0.6
Et	8.2	8.6	-0.3	0.2
Me	8.6	8.6	0.0	0.0
Ph	9.7	9.7	0.0	-1.8
CH_2F	9.9	9.6	0.2	0.9
CH_2OCOMe	10.0	9.1	0.9	1.5
CO_2Me	11.6	10.6	1.0	-0.3
$CH_2NHCOMe$	9.9	8.8	1.1	1.1
OMe	10.4	8.8	1.5	-1.6
CH_2OMe	7.7	5.9	1.8	1.1
OCOMe	14.3	11.7	2.5	0.5
F	16.2	12.2	3.9	1.8

Structures for Exothermicity Calculation

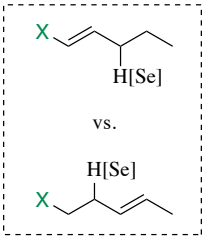

Figure 4.4. Ene $\Delta G^{\ddagger}$ and Exothermicity for Amination in 1,2-Disubstituted Alkenes

We determined that the value of $\Delta\Delta G^{\ddagger}$ ($\Delta G^{\ddagger}$ Near - $\Delta G^{\ddagger}$ Far) tended to be largely positive when an inductively electron-withdrawing group was the X group, thus favoring amination at the site far from X. In contrast, negative $\Delta\Delta G^{\ddagger}$ values were associated with greater selectivity for activation of the allylic C-H bond near the X group, such as when X is CH_2TMS. We next calculated the exothermicity values of the ene reaction to evaluate if the regioselectivity was correlated with the stability of the ene intermediate. Exothermicity was determined by calculating the difference in energy between the ground states of the two possible ene isomers, where the hydrogen group represents selenium. However, a linear regression analysis showed a low correlation coefficient in this case (R^2=0.1).

We therefore completed multivariable regression analysis to describe $\Delta\Delta G^{\ddagger}$ as a function of reaction exothermicity, Taft induction (I) and resonance (R) parameters,[3] and Δ bond dissociation free energy of the allylic C-H bonds (ΔBDFE).[4] The Taft parameters are derived from the Taft equation that describes a linear free energy relationship, which relates reaction rates and equilibrium constants for a range of functional groups. The calculated Taft resonance and induction parameters are used in our models to isolate the inductive and resonance effects of the X substituent in our substrates. ΔBDFE is the difference in free energy of the two types of allylic C-H bonds (near or far to X) and the free energies of those bonds were predicted through a machine learning algorithm.[4] Several models were created with a combination of the variables and the best model exhibited three independent variables and a correlation coefficient of 0.84. (Figure 4.5).

Best model: m1m1d

$\Delta\Delta G^{\ddagger} = -4.2[R] - 0.7[\Delta BDFE] + 1.9[Exothermicity] - 0.4$ **Multiple $R^2 = 0.84$**

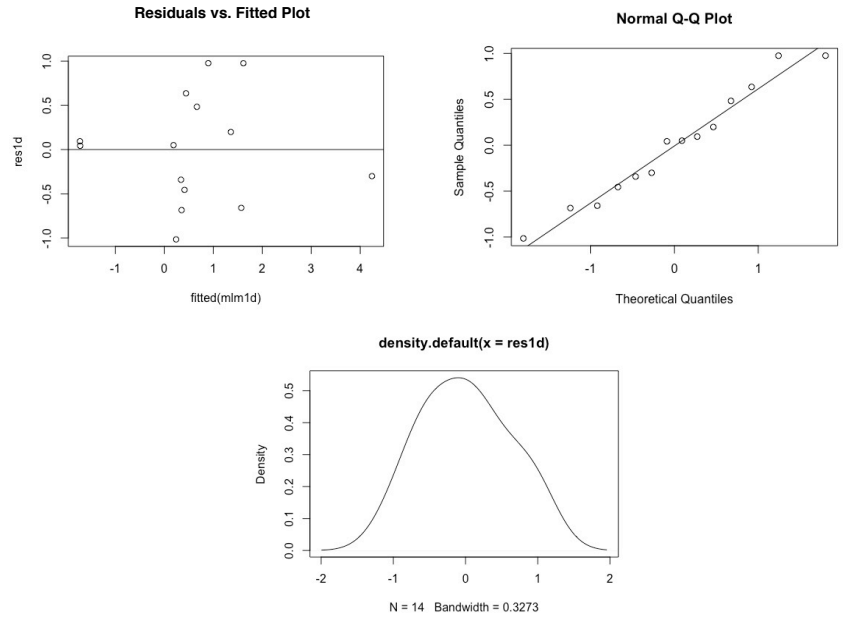

Figure 4.5. Best Multivariable Linear Regression Model for $\Delta\Delta G^{\ddagger}$ and Residual Plots in 1,2-Disubstituted Alkenes

After reviewing the range of the variables, the exothermicity and bond dissociation energy terms had the greatest impact in predicting $\Delta\Delta G^{\ddagger}$. For example, we noted that R ranged to a maximum of ±0.5, so the largest contribution of R to $\Delta\Delta G^{\ddagger}$ could only by ± 2 kcal/mol. Interestingly, the correlation coefficient decreased to 0.6 when the R term was absent from the above model, which suggests a greater importance of the R term to determine $\Delta\Delta G^{\ddagger}$.

We next evaluated the coefficients of each variable to determine their relationship to regioselectivity of amination. The positive coefficient for exothermicity shows that amination will be favored near X (negative $\Delta\Delta G^{\ddagger}$) when formation of the corresponding ene intermediate (for near) is favored (negative exothermicity). This observation shows that stability of the ene intermediates is important for predicting $\Delta\Delta G^{\ddagger}$. Conversely, the negative coefficient for ΔBDFE means this term inversely affects the value of $\Delta\Delta G^{\ddagger}$. Amination is favored near X (negative $\Delta\Delta G^{\ddagger}$) when the near allylic C-H bond requires more energy to break than the far allylic C-H bond (ΔBDFE is positive). This conclusion shows that exothermicity of the entire ene reaction plays a larger role in deciding regioselectivity compared to the energy of breaking a single bond during the ene. The negative coefficient for the Taft parameter shows that electron releasing groups by resonance (negative R) led to amination being favored at the site far from X. A possible mechanism to explain this preference will be presented later in this section.

The residuals of the model were next reviewed to confirm the accuracy of the model and to ensure the errors were normally distributed. The residuals vs. fitted plot showed typically less than 1.0 kcal/mol residual for the model and no significant pattern of residuals with regards to the range of values. The Q-Q plot and density plot also helped confirm a normal distribution of the residuals and thus no significant bias of our mathematical model to predict $\Delta\Delta G^{\ddagger}$.

The role of the Taft resonance parameter was further explored. In amination far from X, we predicted an interaction (via a 5-membered ring) between the X long pair and π^*. Although not resonance, it is likely the strength of this interaction may correlate with the resonance parameter since both involve electron donation of a lone pair. Notably, similar interactions have been observed in the ground states of proteins as well as excited states for small molecules.[6] The X group could be as close as 2.8 Å away from the carbon bearing positive charge (C_{mid}, labeled in blue) in the ene transition state (Figure 4.6).

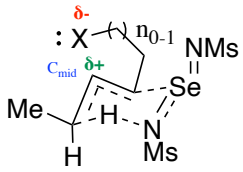

$\Delta G^{\ddagger}$ Far

X	X-Cmid (Å)	X LP to π^* (kcal/mol)
CH_2OMe	2.80	4.2
CH_2OCOMe	2.84	3.0
CO_2Me	2.87	1.6
CH_2F	2.94	1.1
OCOMe	2.95	1.0
$CH_2NHCOMe$	2.98	3.5
CH_2Cl	3.20	3.2

Figure 4.6. Ene Transition State Data for Amination Far in 1,2-Disubstituted Alkenes

For example, the distance between C_{mid} and the methoxy oxygen for X = CH_2OMe is considerably shorter in the transition state (2.8 Å) compared to the ground state of the starting material (3.7 Å). We also estimate the strength of donation of the X lone pair into π^* by completing a second order perturbation theory analysis (of the Fock matrix in NBO basis set) for the ene transition state of interest. The donation was as high as 4.2 kcal/mol in strength and there was a correlation between amination far from X ($\Delta G^{\ddagger}$ far) and donation into π^* with a correlation coefficient of 0.61 (Figure 4.7).

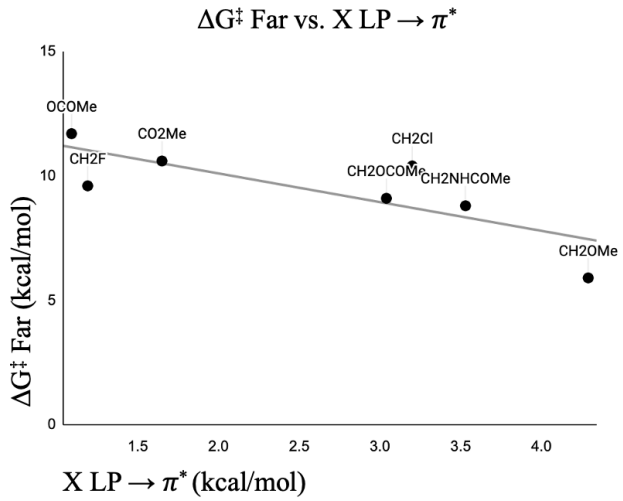

Figure 4.7. $\Delta G^{\ddagger}$ Far vs. X LP → π^*

We also tested a scenario where amination occurred far from X when X = CH_2OMe, but now OMe is anti to the π system and thus donation into π^* is not possible (Figure 4.8).

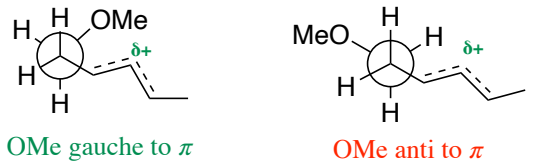

Gauche Transition State more stable than anti by 2.8 kcal/mol

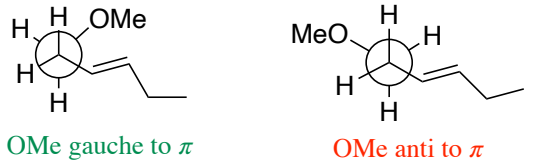

Gauche Ground State more stable than anti by 0.5 kcal/mol

Figure 4.8. Comparing Gauche and Anti for Amination Far in 1,2-Disubstituted Alkenes

We observed an ene barrier that was 2.8 kcal/mol higher in energy than the case when the methoxy lone pair donates into π^*. The ground state corresponding to OMe being gauche to the π system was more stable than the anti-conformation by 0.5 kcal/mol. This observation supports how stabilizing it is to have the gauche relationship in the ene transition state, since positive charge

build-up is larger in magnitude there than in the ground state. We predicted that the donation interaction into π^* is less likely to be significant in the ene transition state when amination occurs near to X ($\Delta G^{\ddagger}$ Near), since a strained 4-membered ring would form. We analyzed the ene for amination near and did not observe donation of the X lone pair into π^*. In these cases, X was typically over 3 Å away from C_{mid} and thus no interaction occurred (Figure 4.9).

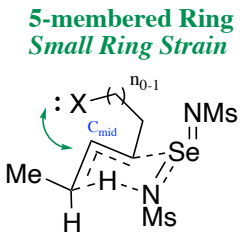

$\Delta G^{\ddagger}$ Far

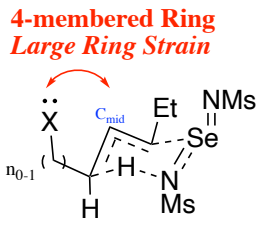

$\Delta G^{\ddagger}$ Near

X	$\Delta G^{\ddagger}$ Far X-Cmid (Å)	$\Delta G^{\ddagger}$ Near X-Cmid (Å)
CH_2OMe	2.80	3.08
CH_2OCOMe	2.84	3.10
CO_2Me	2.87	-
CH_2F	2.94	3.11
OCOMe	2.95	-
$CH_2NHCOMe$	2.98	3.13
CH_2Cl	3.20	3.42

Figure 4.9. X-C_{mid} Bond Distances in Ene for 1,2-Disubstituted Alkenes

Section 4.2.2. *Directing Effects in 1,1-Disubstituted Alkenes*

We investigated 1,1-disubstituted alkenes and determined the ene transition states for amination near the X group. Like the 1,2-disubstituted alkenes, we see that X groups affect the appearance of the transition state. Electron-withdrawing groups led to more concerted transition states with shorter N-H bonds (~ 1.4 Å), whereas electron-releasing X groups led to longer N-H

more concerted

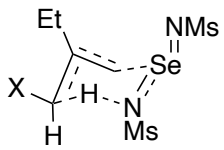

X= EWG

more carbocation character

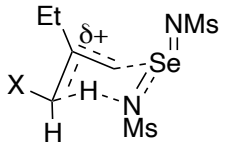

X= EDG

X	N-H (Å)	Allylic C-H (Å)
CF_3	1.47	1.26
CH_2OMe	1.50	1.25
Cl	1.51	1.23
F	1.51	1.25
CH_2OCOMe	1.51	1.25
OCOMe	1.52	1.25
CO_2Me	1.54	1.23
NHCO(Me)	1.54	1.23
Me	1.55	1.24
NMeCOMe	1.55	1.25
TMS	1.57	1.23
OMe	1.60	1.22
CH_2TMS	1.64	1.21

Figure 4.10. Ene Transition State Data for Amination Near X in 1,1-Disubstituted Alkenes

bonds (~ 1.6 Å) and thus more carbocation character (Figure 4.10). We next calculated the ene transition states for amination at each allylic site and the activation ene barriers are summarized below (Figure 4.11).

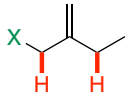

X	ΔG‡ Near (kcal/mol)	ΔG‡ Far (kcal/mol)	ΔΔG‡ (kcal/mol)	Exothermicity (kcal/mol)
CF_3	11.3	10.3	0.9	2.8
CH_2OMe	5.4	3.6	1.7	1.5
Cl	9.7	9.2	0.4	1.2
F	10.2	8.9	1.3	-0.3
CH_2OCOMe	6.4	4.7	1.7	-0.5
OCOMe	8.3	8.0	0.2	-1.3
CO_2Me	7.9	5.6	2.2	-0.9
NHCO(Me)	5.7	1.8	3.9	-3.2
Me	3.9	3.9	0.0	0.0
NMeCOMe	8.6	5.0	3.5	-0.7
TMS	3.7	-2.1	5.9	1.4
OMe	5.4	5.5	0.0	-3.2
CH_2TMS	2.9	3.9	-1.0	-4.7

Structures for Exothermicity Calculation

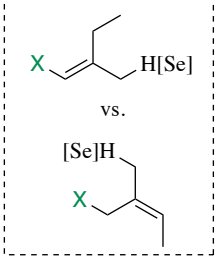

Figure 4.11. Ene ΔG‡ and Exothermicity Data for Amination in 1,1-Disubstituted Alkenes

We observed that the barrier for amination at the site far from X was generally favored and thus $\Delta\Delta G^{\ddagger} \geq 1.0$ kcal/mol. Attempts to build a linear regression model to describe $\Delta\Delta G^{\ddagger}$ were unsuccessful, but we were able to describe $\Delta G^{\ddagger}$ for each site of activation. For amination near X, the best model gave a correlation coefficient of 0.94.

Best model: m1m1cba

$\Delta G^{\ddagger}$ Near = 13.2[I] + 1.3[R] + 0.3[BDFE] - 25.6 **Multiple R^2 = 0.94**

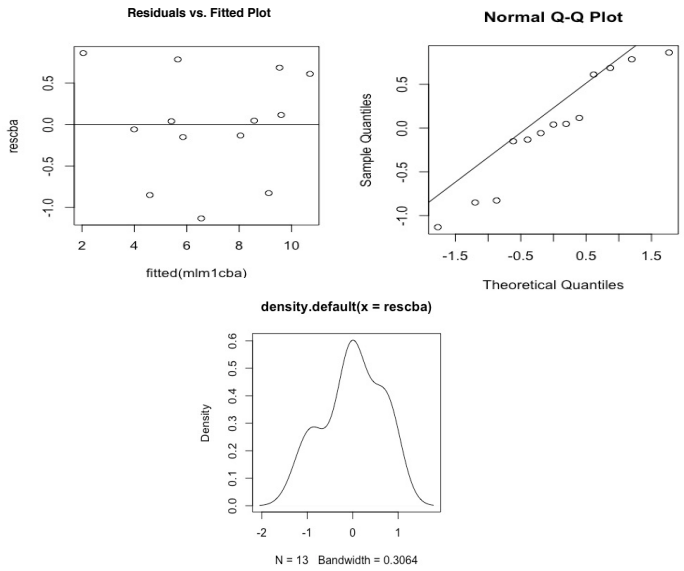

Figure 4.12. Best Multivariable Linear Regression Model for $\Delta G^{\ddagger}$ Near and Residual Plots in 1,1-Disubstituted Alkenes

The linear regression shows that the model requires the induction and resonance Taft parameters as well as the bond dissociation energy for the allylic C-H bond (BDFE) being abstracted (Figure 4.12). The variable that was the most important was BDFE, followed by the induction term. The importance of the variables was ranked by evaluating the magnitude of the variable across the data range, which was done by multiplying the coefficient assigned to the variable in the model by the sample quantities for that variable (determined computationally). The positive coefficient for the induction term means that X groups that are electron-withdrawing led to higher $\Delta G^{\ddagger}$ values. The negative coefficient in front of the resonance parameter means electron-

releasing groups decreased $\Delta G^{\ddagger}$. For a large BDFE of the allylic C-H bond, $\Delta G^{\ddagger}$ increased for the ene reaction.

Analysis of the residuals for this model showed them to be lower than 0.5 kcal/mol, but there are cases the residuals could be as high as 1.0 kcal/mol. Most of the residuals are normally distributed and small in magnitude.

A model was next produced to predict $\Delta G^{\ddagger}$ for amination far from X (Figure 4.13)

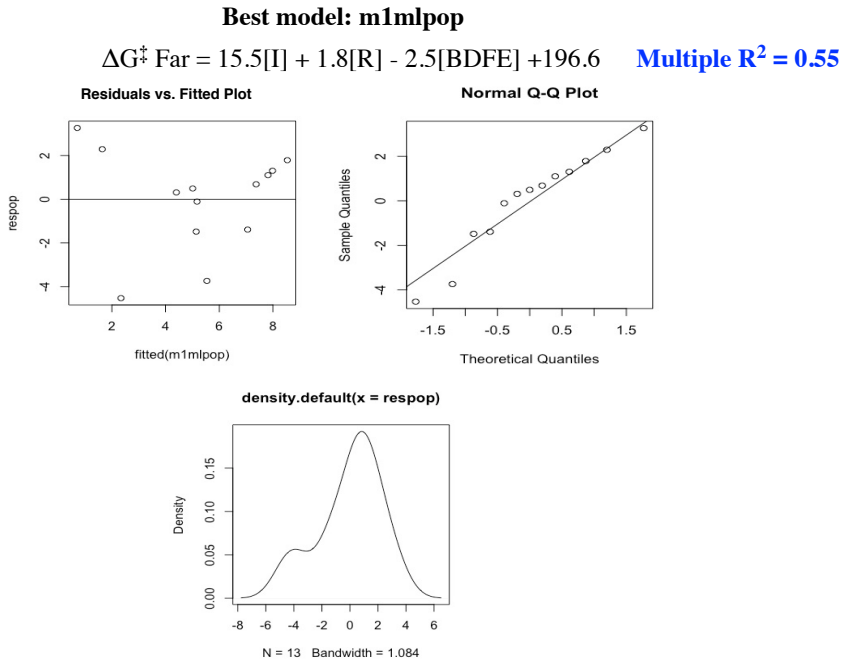

Figure 4.13. Best Multivariable Linear Regression Model for $\Delta G^{\ddagger}$ Far and Residual Plots in 1,1-Disubstituted Alkenes

and the best model led to a correlation coefficient of 0.55. Like $\Delta G^{\ddagger}$ for amination near, the model for $\Delta G^{\ddagger}$ at the far site requires the inductive and resonance Taft parameters and bond dissociation free energy for the allylic C-H. We observed that the bond dissociation free energy had the largest influence followed by the Taft induction term in predicting $\Delta G^{\ddagger}$ far. The model equation exhibits the same variables and sign of the coefficients as the model for $\Delta G^{\ddagger}$ near, so the interpretations of variables is consistent with both cases. The residuals although could be large in these cases (~2 kcal/mol) and there was a minor tailing of the residuals.

Section 4.2.3. *Effect of Vinyl-X on Ene Reaction*

Our group previously showed that alkenes containing X groups at the vinyl position are applicable in our allylic amination chemistry. In this respect, our group evaluated vinylsilanes, vinylboronate esters, vinylphosphates, vinylhalides, vinylsulfonates, and vinylesters. A computational study was conducted to calculate $\Delta G^{\ddagger}$ of the ene reaction and to better understand what effects the substituents induce (Figure 4.14).

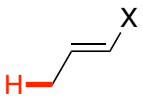

X	$\Delta G^{\ddagger}$ (kcal/mol)	Se-C (Å)
TMS	10.7	2.13
OH	11.7	2.52
CH_3	11.8	2.25
H	12.9	2.21
OCH_3	13.7	2.51
SiH_3	14.0	2.22
SMe	15.2	2.39
$B(OH)_2$	15.3	2.20
PH_2	15.7	2.25
$PO(OH)_2$	15.7	2.34
SH	16.6	2.35
$O{=}CCH_3$	17.9	2.36
CHO	19.7	2.40
CO_2H	19.8	2.38
Br	20.2	2.33
F	20.6	2.38
Cl	20.8	2.35
CF_3	23.1	2.37
CCl_3	23.1	2.39
CBr_3	23.4	2.40

Figure 4.14. Ene Transition State Data for Amination in Vinyl-X

A mathematical model to predict $\Delta G^{\ddagger}$ in the ene reaction of these substrates would be useful to identify what substrates exhibit the lowest ene barrier and thus will be suitable for our selenium chemistry. We first calculated the ene transition states for 20 different vinyl-X alkenes that exhibited a diverse range of electronic character. In general, we observed a trend where X substituents that result in lower activation barriers also showed shorter Se-C distances (~ 2.2 Å) in

the ene transition state. A short Se-C distance can be associated with a more asynchronous ene mechanism, the closer approach of Se leading to advanced bond formation of the Se-C bond and delayed breaking of the allylic C-H bond.

A linear regression model was next determined using the Taft inductive and resonance parameters and we observed a high correlation coefficient of 0.74 (Figure 4.15). This model only

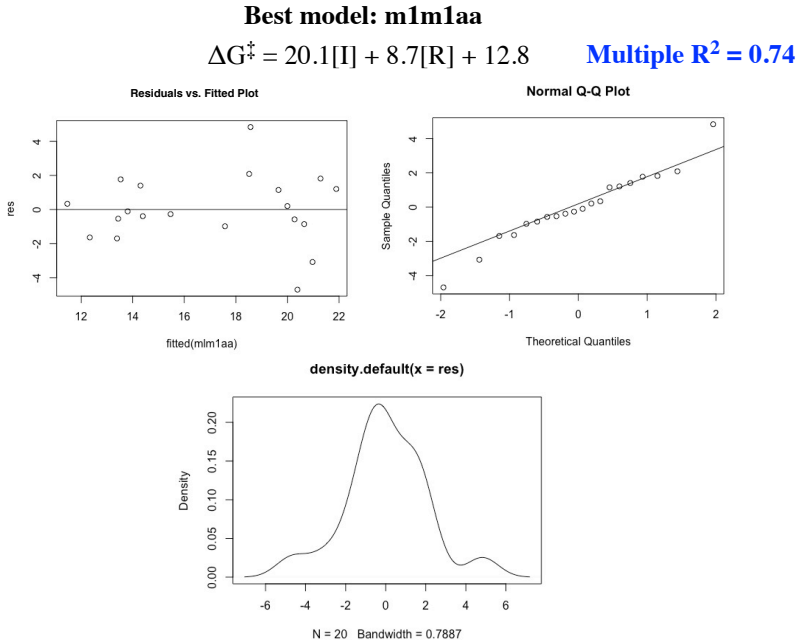

Figure 4.15. Best Multivariable Linear Regression Model for $\Delta G^{\ddagger}$ and Residual Plots in Vinyl-X

utilizes the Taft induction and resonance parameters and the residuals appear to be normally distributed. The induction parameter had the largest influence of predicting $\Delta G^{\ddagger}$ in these cases, since the coefficient is over twice the magnitude for the resonance parameter and the range of the induction variable is thus larger. The positive coefficient for the induction term means electron-withdrawing groups led to higher values for $\Delta G^{\ddagger}$. Similarly, a positive coefficient for the resonance term means electron-withdrawing groups via induction led to higher $\Delta G^{\ddagger}$ too.

Section 3: CONCLUSION

In conclusion, we determined the ene transition states for amination in 1,2-disubstituted alkenes, 1,1-disubstituted alkenes, and vinyl-X compounds. Multivariable linear regression models were presented to predict $\Delta G^{\ddagger}$ or $\Delta\Delta G^{\ddagger}$ in these cases. For the 1,2- and 1,1-disubstituted alkenes and vinyl-X compounds, more carbocation character was observed on the central carbon in the ene transition states when X was an electron-releasing group. We determined that the exothermicity and bond dissociation energy of the allylic C-H bonds had the largest effect in predicting $\Delta\Delta G^{\ddagger}$ for 1,2-disubstituted alkenes. The resonance parameter was represented in the model too perhaps because of an interaction between the lone pair of the X group with the partial positive charge building in the ene transition state (Figure 4.16).

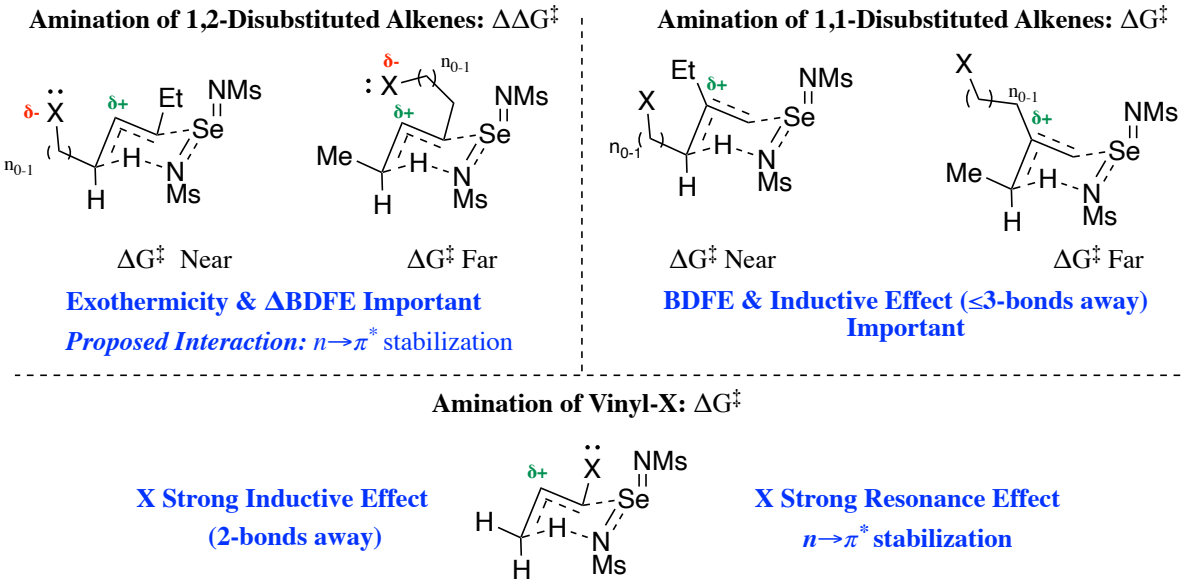

Figure 4.16. Proposed Interpretation of Regression Models for Ene $\Delta G^{\ddagger}$ and $\Delta\Delta G^{\ddagger}$

For 1,1-disubstituted alkenes, the bond dissociation free energy of the allylic C-H bond and induction parameter played a large role in predicting $\Delta G^{\ddagger}$. We can interpret the importance of the induction parameter by how the X group is considerably close to the partial positive charge building in the transition state (2-3 bonds away). The ability of the X group to inductively stabilize or destabilize that positive charge can significantly affect $\Delta G^{\ddagger}$. The X group can also affect the

acidity of the allylic C-H bond that is abstracted in the reaction, which alludes to the importance of the bond dissociation free energy term.

The regression model to describe $\Delta G^{\ddagger}$ for vinyl-X relied on the Taft induction and resonance parameters. We hypothesize that the inductive effect exhibits the largest influence on the ene reaction barrier because of the X group's enhanced proximity to the positive charge (2 bonds away). However, a resonance effect via donation of the X group lone pair into π^* on the adjacent carbons could affect the positive charge in the transition state as well.

Section 4: EXPERIMENTAL

Section 4.4.1. *General Procedures and Methods*

DFT calculations were performed using the Gaussian-16 software package. Structures were optimized at the wB97-XD/6-311++G(d,p) level of theory, using the PCM model with CH_2Cl_2 as solvent. Frequency calculations were performed on all structures and enthalpies and free energies were calculated using the harmonic approximation at standard state (1 M concentration). Free energies of activation have been adjusted and recorded for 0.04 M concentration to better reflect the experimental conditions. All structures had zero negative frequencies, and the transition state had one negative frequency whose motions corresponded to the expected reaction coordinate.

Section 4.4.2. *Transition States, Intermediates, & Statistics*

Gaussian files are in Michael Group OneDrive/Berman/Thesis Calculation Files/12alkenes/Transition States. Table 4.1 conveys details of the ene transition states and the name of the corresponding Gaussian file for reactions of the 1,2-disubstituted alkenes studied.

Table 4.1. Filenames for Ene Transition States for Amination of 1,2-Disubstitued Alkenes[a]

X Group	Amination Site (Near or Far to X)	Filename (.log ending)
$CH2B(OCH_2)_2$	Near	12ch2bpinnearberny2222022
$CH2B(OCH_2)_2$	Far	12ch2bpinoppbernyredo2222022
CH_2CF_3	Near	12ch2cf3bernynear2222022
CH_2CF_3	Far	12ch2cf3oppdownberny312022nbo
CH_2CH_3	Near	12ch2ch3bernyrt2222022
CH_2CH_3	Far	12ch2ch3oppberny2222022
CH_2Cl	Near	12ch2clnearbernyrt2222022nbo
CH_2Cl	Far	12ch2cloppberny1242022nbo
CH_2F	Near	12ch2fnearbernyrt2222022nbo
CH_2F	Far	12ch2foppberny1302022nbo
$CH_2NHCOMe$	Near	12ch2nhcomenearbernyrttry2222022nbo
$CH_2NHCOMe$	Far	12ch2nhcomeoppberny2222022nbo
CH_2OCOMe	Near	12ch2ocomenearbernyrt2222022nbo
CH_2OCOMe	Far	12ch2ocomeoppberny2212022nbo
CH_2OMe	Near	12ch2omebernyrt2222022trynbo
CH_2OMe	Far	12ch2omeoppberny1302022nbo
CH_2OMe	Far (now CH_2OMe anti to π system)	12ch2omeanti522022
CH_2TMS	Near	12ch2tmsnearbernyrt2222022
CH_2TMS	Far	12ch2tmsoppbernyredo2222022
CH_3	Near	12ch3nearbernyredo2222022
CH_3	Far	12ch3oppberny2222022
CO_2Me	Near	12co2menearbernyrt2222022
CO_2Me	Far	12co2meoppberny1302022nbo

F	Near	12fberny1162022nbo
F	Far	12foppbernyredone2222022
OCOMe	Near	12ocomeberny2212022
OCOMe	Far	12ocomeberny312022nbo
OMe	Near	12omeberny1252022nbo
OMe	Far	12omeoppberny1302022
Ph	Near	12phnearberny352022
Ph	Far	12phfarrberny342022
TMS	Near	12alphasime3berny272022
TMS	Far	12alphasime3oppredoberny2222022

[a]Statistical analysis did not include the following X groups: $CH_2B(OCH_2)_2$, TMS.

Gaussian files are in Michael Group OneDrive/Berman/Thesis Calculation Files/12alkenes/Intermediates. Table 4.2 conveys details of the simplified ene intermediates and the name of the corresponding Gaussian file for reactions of the 1,2-disubstituted alkenes studied.

Table 4.2. Filenames for Simplified Ene Intermediates for Amination of 1,2-Disubstitued Alkenes[a]

X Group	**Amination Site (Near or Far to X)**	**Filename (.log ending)**
$CH2B(OCH_2)_2$	Near	12ch2bpinprodnear2142022
$CH2B(OCH_2)_2$	Far	12ch2bpinprodfar2142022
CH_2CF_3	Near	12ch2cf3eneprodnear242022
CH_2CF_3	Far	12ch2cf3prodfar2142022
CH_2CH_3	Near	12ch2ch3eneprodnear232022
CH_2CH_3	Far	12ch2ch2ch3prodfar2142022
CH_2Cl	Near	12ch2cleneprodnear252022
CH_2Cl	Far	12ch2clprodfar2142022
CH_2F	Near	12ch2feneprodnear232022
CH_2F	Far	12ch2fprodfaropt2142022
$CH_2NHCOMe$	Near	12ch2nhcomeprodnear292022

$CH_2NHCOMe$	Far	12ch2nhcomeprodfar2142022
CH_2OCOMe	Near	12ch2ocomeprodnear292022
CH_2OCOMe	Far	12ch2ocomeprodfar292022
CH_2OMe	Near	12ch2omeeneprodnear242022
CH_2OMe	Far	12ch2omeprodfar2152022
CH_2TMS	Near	12ch2tmsprodnear2142022
CH_2TMS	Far	12ch2tmsprodfar2142022
CH_3	Near	12meeneprodnearfar272022copy
CH_3	Far	12meeneprodnearfar272022
CO_2Me	Near	12co2meprodnear292022
CO_2Me	Far	12co2meprodfar292022
F	Near	12feneprodnear252022
F	Far	12alphafprodfar292022
OCOMe	Near	12ocomeprodnear2282022
OCOMe	Far	12ocomeprodfar2282022
OMe	Near	12omeprodnear2142022
OMe	Far	12omeprodfar2142022
Ph	Near	12phenenear352022
Ph	Far	12phfarene352022
TMS	Near	12alphatmsprodnear292022
TMS	Far	12alphatmsprodenefar292022

[a]Statistical analysss did not include the following X groups: $CH_2B(OCH_2)_2$, TMS.

Gaussian files are in Michael Group OneDrive/Berman/Thesis Calculation Files/12alkenes/Starting Alkenes. Table 4.3 conveys details of the starting alkenes and the name of the corresponding Gaussian file for reactions of the 1,2-disubstituted alkenes studied.

Table 4.3. Filenames for Starting Alkenes for Amination of 1,2-Disubstitued Alkenes

X Group	**Filename (.log ending)**

$CH2B(OCH_2)_2$	12ch2bpinsmopt1252022
CH_2CF_3	12ch2cf3sm492022
CH_2CH_3	12ch3smopt132022nbo
CH_2Cl	12clsmopt1122022nbo
CH_2F	12ch2fprodenefar232022
$CH_2NHCOMe$	12ncomesmopt1242022
CH_2OCOMe	12ocomesmoptredo1242022
CH_2OMe	12omesmoptnbo132022
CH_2OMe (OMe anti to π)	12ch2omesma5102022
CH_2OMe (OMe gauche to π)	12ch2omesmg5102022
CH_2TMS	12ch2tmssmopt1252022
CH_3	12ch3smopt1252022
CO_2Me	12estersmopt1232022
F	12fsmopt2142022
OCOMe	12ocomesmnear2282022
OMe	12omesmopt1252022
Ph	12phsmopt462022
TMS	12alphatmssmopt292022

R Studio and Excel files for the statistics completed for 1,2-alkenes are in Michael Group OneDrive/Berman/Thesis Calculation Files/Statistical Analysis/12 alkenes and are summarized in Table 4.4.

Table 4.4. Filenames for Statistical Analysis of 1,2-Disubstitued Alkenes

File Description	**Filename**
Excel sheet with the data used in R	onetwoalkenesabb5v.csv
Excel sheet with the data and correlation plot for donation into π^*	11and12alkenedata_4252022Edited
R Studio file with statistical models	12alkeneanalysis.R

Gaussian files are in Michael Group OneDrive/Berman/Thesis Calculation Files/11alkenes/Transition States. Table 4.5 conveys details of the ene transition states and the name of the corresponding Gaussian file for reactions of the 1,1-disubstituted alkenes studied.

Table 4.5. Filenames for Ene Transition States for Amination of 1,1-Disubstitued Alkenes[a]

X Group	Amination Site (Near or Far to X)	Filename (.log ending)
$CH2B(OCH_2)_2$	Near	ch2bbpinleftberny1172022trynbo
$CH2B(OCH_2)_2$	Far	ch2bbpinberny1172022nbo
CF_3	Near	cf3berny11272021mnbo11292021m
CF_3	Far	cccf3berny12202021mnbo
$B(OCH_2)_2$	Near	bbpinberny1172022nbo
$B(OCH_2)_2$	Far	bpinoppbernytry1202022nbo
CH_2OCOMe	Near	ch2ocomeberny222022nbo
CH_2OCOMe	Far	cch2ocomeoppberny232022
CH_2OMe	Near	ch2omeberny222022nbo
CH_2OMe	Far	cch2omeoppberny222022
CH_2TMS	Near	csich3berny12102021mnbo
CH_2TMS	Far	ccsime3berny172022nbo
CH_3	Near	mebernyredo12152021mnbo
CH_3	Far	ccch3berny12202021mnbo
Cl	Near	clberny11212021mnbo11212021m
Cl	Far	ccclberny12202021mnbo
CO_2Me	Near	co2rberny11272021mnbo11292021m
CO_2Me	Far	ccco2rberny12202021mnbo
F	Near	fbernyredo11212021mnbo11212021m
F	Far	ccfrberny1262021mnbo1262021m
$NMeCO(CH_2)_3$	Near	11lactamberny2142022
$NMeCO(CH_2)_3$	Far	lactamoppredoberny2202022

NHCOMe	Near	ncorbernytry1262022nbogood
NHCOMe	Far	ccncorredoberny12222021mnbo
NMeCOMe	Near	nmecorberny272022
NMeCOMe	Far	ccnmecorberny272022
OCOMe	Near	ocorbernyredone1242022
OCOMe	Far	ccocorberny12232021mnbo
OMe	Near	omeberny11212021mnbo11212021m
OMe	Far	ccometryberny12202021mnbo
SiH_3	Near	sih3berny1232021mberny1262021m
SiH_3	Far	ccsih3berny12202021mnbo
TMS	Near	sich3berny1102022nbo
TMS	Far	ccsich3berny1162022nbo
$N(COCH_2)_2$	Near	11succinimidenearberny2282022
$N(COCH_2)_2$	Far	succinimideoppberny332022

[a]Statistical analysis did not include $B(OCH_2)_2$, $N(COCH_2)_2$ or SiH_3.

Gaussian files are in Michael Group OneDrive/Berman/Thesis Calculation Files/11alkenes/Transition States. Table 4.6 conveys details of the simplified ene intermediates and the name of the corresponding Gaussian file for reactions of the 1,1-disubstituted alkenes studied.

Table 4.6. Filenames for Simplified Ene Intermediates for Amination of 1,1-Disubstitued Alkenes

X Group	**Amination Site (Near or Far to X)**	**Filename (.log ending)**
$CH2B(OCH_2)_2$	Near	pseudoch2bpinene1172022
$CH2B(OCH_2)_2$	Far	ch2bpinoppenert2202022
CF_3	Near	pseudocf3prodopt12132021m
CF_3	Far	11enecf3rt2202022
$B(OCH_2)_2$	Near	pseudobpinene1172022
$B(OCH_2)_2$	Far	11enebpinopprt2202022

CH_2OCOMe	Near	pseudoch2ocomeprod242022
CH_2OCOMe	Far	11ch2ocomeprodrtnfar2202022
CH_2OMe	Near	pseudo11ch2omeprodopt222022
CH_2OMe	Far	11ch2omeprodrtfar2202022
CH_2TMS	Near	pseudosich3ch2prodopt12132021m
CH_2TMS	Far	ch2tmsoppene1222022
CH_3	Near	pseudomeeneprod12152021m
CH_3	Far	11enech3rtfar2202022
Cl	Near	pseudoclprodopt12132021m
Cl	Far	11eneoppb1172022
CO_2Me	Near	pseudoco2rcbprodopt12132021m
CO_2Me	Far	11eneco2mertopp2202022
F	Near	pseudofprodopt12132021m
F	Far	11feneopprt2202022
$NMeCO(CH_2)_3$	Near	11lactamprodnear442022
$NMeCO(CH_2)_3$	Far	11lactamprodrtfar2202022
NHCOMe	Near	pseudoncorprodopt12132021m
NHCOMe	Far	11enencorfarrt2202022
NMeCOMe	Near	nmecoreneprodnear272022
NMeCOMe	Far	nmecorenertprodfar2202022
OCOMe	Near	pseudoco2rprodopt12132021m
OCOMe	Far	11ocomeeneprodfar442022
OMe	Near	omeene1222022
OMe	Far	11eneomeprodrtfar2202022
SiH_3	Near	pseudosih3prodopt12132021m
SiH_3	Far	11enesih3prodfar432022
TMS	Near	pseudosime3prodopt222022
TMS	Far	11enesime3prodfarrt2202022
$N(COCH_2)_2$	Near	11succinimideprodnear2282022
$N(COCH_2)_2$	Far	11succinimideprodfar2282022

[a]Statistical analysis did not include $B(OCH_2)_2$, $N(COCH_2)_2$ or SiH_3.

Gaussian files are in Michael Group OneDrive/Berman/Thesis Calculation Files/12alkenes/Starting Alkenes. Table 4.7 conveys details of the starting alkenes and the name of the corresponding Gaussian file for reactions of the 1,1-disubstituted alkenes studied.

Table 4.7. Filenames for Starting Alkenes for Amination of 1,1-Disubstitued Alkenes

X Group	Filename (.log ending)
$CH2B(OCH_2)_2$	ch2bpinopt1172022
CF_3	cf3redonbo1262021m
$B(OCH_2)_2$	bpinoptsm1182022
CH_2OCOMe	11ch2ocomesmopt232022
CH_2OMe	11ch2omesmopt222022nbo
CH_2TMS	sime3ch2opt12132021m
CH_3	mesmopt12152021m
Cl	clopt11162021mnbo
CO_2Me	co2metryopt11172021mnbo
F	fopt11162021mnbo
$NMeCO(CH_2)_3$	11lactamsm2282022
NHCOMe	ncoropt12132021m
NMeCOMe	nmecoropt272022
OCOMe	ocorredonbo1262021m
OMe	omeopt11162021mnbo
SiH_3	sih3redonbo1262021m
TMS	sich3nbo1112022
$N(COCH_2)_2$	11succinimidesmtry2282022

R Studio and Excel files for the statistics completed for 1,1-alkenes are in Michael Group OneDrive/Berman/Thesis Calculation Files/Statistical Analysis/11 alkenes and are summarized in Table 4.8.

Table 4.8. Filenames for Statistical Analysis of 1,1-Disubstitued Alkenes

File Description	Filename
Excel sheet with the data for R	oneonnealkenesabb5vfinalcsv
Excel sheet with all the data	11and12alkenedata_4252022Edited
R Studio file with statistical models	11alkenesfinal.R

Gaussian files are in Michael Group OneDrive/Berman/Thesis Calculation Files/Vinyl-X /Transition States. Table 4.9 conveys details of the ene transition states and the name of the corresponding Gaussian file for reactions of the Vinyl-X studied.

Table 4.9. Filenames for Ene Transition States for Amination of Vinyl-X[a]

X Group	Filename (.log ending)
BH_2	bh2tsnbo7102021
CH_3	Test_F_DFT_nbo7102021
SiH_3	Test_c_calcfc_DFT_nbo7102021
PH_2	vinylptsnbo7102021
Br	VinylBr_dist_3122021_nbo7102021
F	vinylfberny742021_nbo7102021
OH	ohtsnbo7102921
H	vinylhbernyok7142021_nbo7152021
SH	vinylsqst27142021_nbo7152021
CF_3	cf3eneberny8262021_nbo8272021
$B(OH)_2$	boh2eneberny8272021adjust_nbo8282021

$Si(OH)_3$	sioh3eneberny8272021_nbo8282021
CHO	vinylaldberny8282021_nbo8282021
OCH_3	vinylcomeqst28282021_nbo8282021
$O{=}CCH_3$	vinylketberny8282021_nbo8282021
CBr_3	cbr3eneberny8282021_nbo8282021
CO_2H	vinylestberny8282021_nbo8282021
$PO(OH)_2$	vinylphosacberny8282021_nbo8292021
$SiMe_3$	tmseneberny922021_nbo922021
SMe	vinylsmeberny932021_nbo932021
BMe_2	bme2berny932021_nbo932021
CCl_3	ccl3berny952021_nbo952021
Cl	vinylclberny952021_nbo952021

[a]Statistical analysis did not include the following X groups: BH_2, BMe_2, and $Si(OH)_3$.

Gaussian files are in Michael Group OneDrive/Berman/Thesis Calculation Files/Vinyl-X /Starting Alkenes & Selenium Diimide. Table 4.10 conveys details of the ground states and the name of the corresponding Gaussian file for reactions of the Vinyl-X studied.

Table 4.10. Filenames for Starting Alkenes and Selenium Diimide for Amination of Vinyl-X[a]

X Group	**Filename (.log ending)**
BH_2	bh2opt6302021_nbo7122021
CH_3	2buteneopt7102021_nbo7132021
SiH_3	SiSM_DFT_REDO
PH_2	vinylpopt7122021
Br	vinylbropt7102021_nbo7132021
F	vinylfopt722021_nbo7122021
OH	oh2eneopt6302021_nbo7122021
H	vinylhopt7142021
SH	vinylsopt7142021

CF_3	vinylcf3optnbo8272021
$B(OH)_2$	vinylbohopt8282021
$Si(OH)_3$	vinylsioh3opt8282021_nbo8282021
CHO	vinylaldopt8272021
OCH_3	vinylcomeopt8282021
$O{=}CCH_3$	vinylketopt8282021
CBr_3	vinylcbr3opt8272021
CO_2H	vinylacidopt8292021
$PO(OH)_2$	vinylphosacidopt8292021
$SiMe_3$	tmssmopt922021
SMe	vinylsmesmopt932021
BMe_2	bmesmopt932021
CCl_3	vinylcl3opt952021
Cl	vinylclopt952021
Selenium Diimide (anti-anti)	diimideantiantiopt612021
Selenium Diimide (syn-anti)	MethaneSulfonate_diimide_opt_freq

[a]Statistical analysis did not include the following X groups: BH_2, BMe_2, and $Si(OH)_3$.

R Studio and Excel files for the statistics completed for Vinyl-X are in Michael Group OneDrive/Berman/Thesis Calculation Files/Statistical Analysis/Vinyl-X and are summarized in Table 4.11.

Table 4.11. Filenames for Statistical Analysis of Vinyl-X[1]

File Description	**Filename**
Excel sheet with the data	xpropenes.csv
R Studio file with statistical models	xpropenesanalysis.R

REFERENCES FOR CHAPTER 4

[1] Lei, H; Rovis, T. A. *Nat. Chem.* **2020,** *12,* 725-731.

[2] Maloney, T. P.; Dohoda, A. F.; Zhu, A. C.; Michael, F. E. *Chem. Sci.* **2022,** *13,* 2121-2127.

[3] Hannsch, C.; Leo, A.; Taft, R. W. *Chem. Rev.* **1991,** *91,* 165-195.

[4] (a) National Renewable Energy Laboratory ALFABET. https://bde.ml.nrel.gov/. (b) St. John, P.C.; Guan, Y.; Kim, Y.; Kim, S.; and Paton, R.S. *Nat Commun* **2020,** *11,* 2328-2340. (c) St. John, P.C.; Guan, Y.; Kim, Y.; Etz, B.D.; Kim S.; and Paton, R.S. *Sci Data* **2020,** *7,* 244-250.

[5] (a) Pederes, G. D.; Jorgensen, W. L. *J. Org. Chem.* **1992,** *57,* 1904-1916. (b) Fernández, I.; Bickelhaupt, F. M. *J. Comput. Chem.* **2012,** *33,* 509-516.

[6] (a) Vik, E. C.; Pellechia, P. J.; Shimizu, K. D. *J. Am. Chem. Soc.* **2019,** *141,* 16579-16583. (b) Hodges, J. A.; Raines, R. T. *Org. Lett.* **2006,** *8*, 4695−4697. (c) Choudhary, A.; Gandla, D.; Krow, G. R.; Raines, R. T. *J. Am. Chem. Soc.* **2009,** *131,* 7244−7246. (d) Newberry, R. W.; Raines, R. T. *Acc. Chem. Res.* **2017,** *50,* 1838−1846.

Chapter 5. FACTORS GOVERNING NOVEL REGIOSELECTIVITY IN ENE OF ALLYLIC C-H AMINATION

Section 1: INTRODUCTION

The regiochemical outcome for the ene reaction involving SeO_2 has been well studied[1] and can thus be a first approximation to predict regioselectivity in our allylic amination reaction. In general, development of positive charge at the internal vinyl carbon (C_{mid}) is critical to this analysis. Abstraction of the allylic C-H bond occurs at the site that forms the most stable ene intermediate, this is generally the allylic C-H at the more substituted end of the alkene (Figure 5.1).[1]

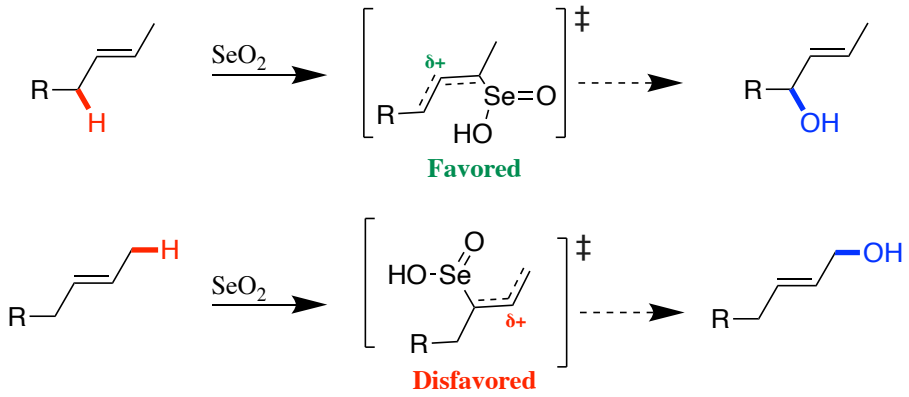

Figure 5.1. General Regioselectivity in SeO_2 Oxidations of Aliphatic Alkenes

In this respect, regioselectivity is driven by electronic considerations. However, steric properties at the allylic site are also important and a general trend is thus observed (CH_2 > CH ~ CH_3). This prediction system becomes less informative when multiple allylic C-H bonds are available, and they are in similar chemical environments.

To this end, our group's initial report on allylic amination showed unique examples of regioselectivity when cyclic terpenes were utilized as substates.[2] Notable examples include the amination products derived from methyl jasmonate and δ-damascone (Figure 5.2).

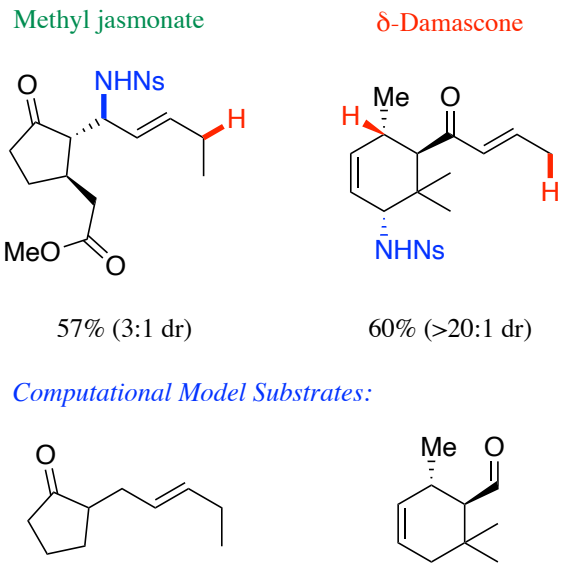

Figure 5.2. Special Cases of Regioselective C-H Amination of Terpenes

We noticed in both cases that chemically similar allylic C-H bonds are available (occupying 2º aliphatic positions), but only one was abstracted. In the case of methyl jasmonate, we hypothesized that the carbonyl oxygen could affect the stability of the ene transition state. Perhaps the lone pair of the oxygen interacts with the internal vinyl carbon bearing positive charge and this interaction imposes conformational constraints on the transition state. This feature could then make abstraction of the allylic C-H bond regioselective. In terms of δ-damascone, we questioned whether building 1,3-allylic strain between the ketone and adjacent methyl group could be consequential in regioselectivity.

By employing a computational study, we were motivated to elucidate possible reasons for regioselective allylic C-H bond activation in these cases. We utilized the model substrates shown in Figure 5.2 for this study. For methyl jasmonate, the starting alkene stereochemistry is *cis,* but

we will use a *trans* double bond in our model compound to simplify our calculations. Our findings could enable us to formulate trends in allylic C-H bond reactivity in these special situations to make our amination method more user-friendly in the synthetic field.

Section 2: RESULTS & DISCUSSION

Section 5.2.1. *Ene Transition State Analysis of Methyl Jasmonate*

We began evaluating the ene transition states corresponding to abstraction of either of the allylic C-H bonds in methyl jasmonate (Figure 5.3).

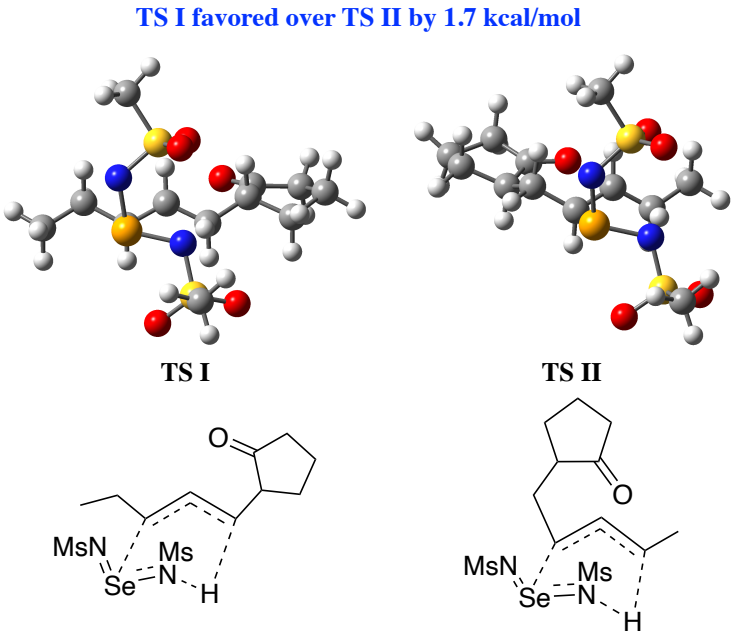

Figure 5.3. Ene Transition States for Methyl Jasmonate

Transition state I (TS I) corresponds to abstraction of the C-H bond β to the carbonyl, while transition state II (TS II) corresponds to the C-H bond ε to the carbonyl. These transition states differed by 1.7 kcal/mol and TS I was favored, which agreed with our experimental findings.

We observed a substantially shorter distance between the carbonyl oxygen and the internal vinyl carbon (O-C_{mid}.) in TS II (Figure 5.4). This short distance can be associated with an interaction

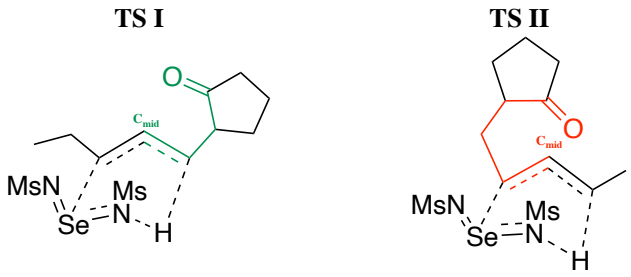

Transition States	O-C_{mid} Distance (Å)	LP O → π^* (kcal/mol)
TS I	3.05	2.17
TS II	2.62	10.71
Δ (TS I - TS II)	0.43	8.54

Figure 5.4. Comparison of Ene Transition States for Methyl Jasmonate

between the carbonyl oxygen and the internal vinyl carbon, where donation of the X lone pair into π^* is 10 kcal/mol after completing a second order perturbation theory analysis (of the Fock matrix in NBO basis set). Although this interaction appears to be large in magnitude, NBO calculations tend to be larger than the actual energy of an interaction by 3 or 4 times. The fact that TS II exhibits the interaction more strongly than TS I is a significant observation, but this electronic interaction overall forces a 6-membered half-chair conformation in that transition state (shown in red) that leads to destabilizing eclipsing interactions. The favored transition state (TS I) could be favored because this electronic event is smaller in magnitude and a less strained 5-membered ring conformation is formed.

Section 5.2.2. *Ene Transition State Analysis of δ-Damascone*

We extended our analysis to a model compound of δ-damascone and we determined the two possible ene transition states (Figure 5.5).

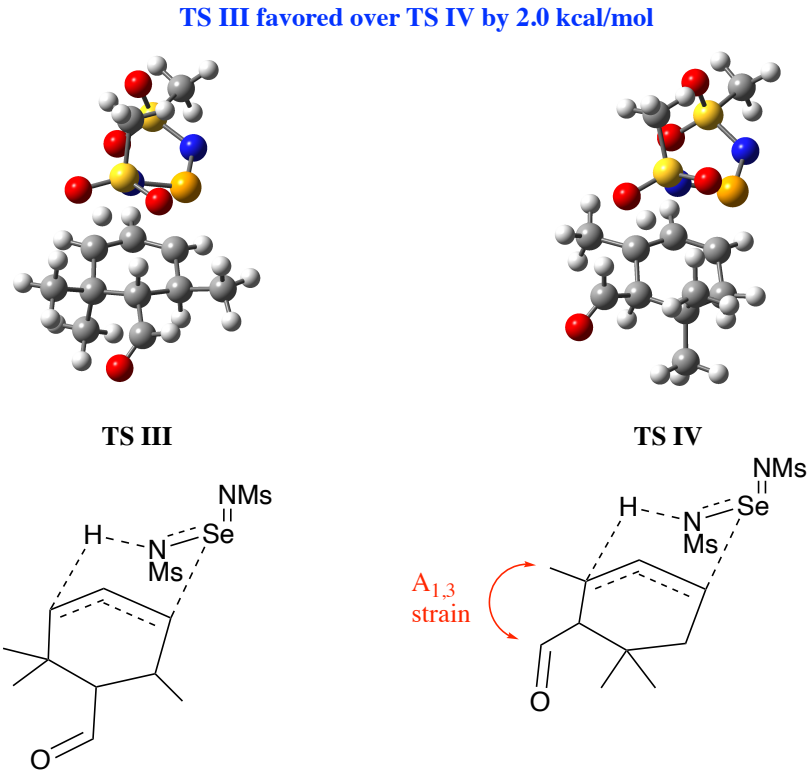

Figure 5.5. Ene Transition States for δ-Damascone

Transition state III (TS III) represents amination at the site adjacent to the gem-dimethyl group, whereas transition state IV (TS IV) exhibits amination *β* to the aldehyde. We observed that TS III was favored over TS IV by 2.0 kcal/mol, which agreed with our experimental findings. A possible explanation for the regioselectivity is that activation at the site near the aldehyde forces the methyl group coplanar to the aldehyde. A consequence of this regiochemical path is thus 1,3-allylic strain is greater in magnitude at the site of C-H abstraction in TS IV, since TS III exhibits this strain between a hydrogen and smaller methyl group instead. The cyclic substrate forces a *cis* stereochemistry of the double bond, which likely decreases conformational flexibility in the ene transition state. This feature contributed to the enhanced consequences for 1,3-allylic strain during

the ene reaction, which we have reported previously in amination of *Z*-alkenes.[3] Further precedence for this explanation can be found in how 1,3-allylic strain has been implicated in stereochemical and regiochemical outcomes in several transformations.[4,5]

Section 3: CONCLUSION

We studied the ene transition states concerning allylic amination of cyclic terpenes. In the case of methyl jasmonate, an unstable half-chair conformation was observed in the disfavored ene transition state. This conformation could be a consequence of a strong interaction between a lone pair of electrons on the carbonyl oxygen and the electrophilic internal vinyl carbon. When δ-damascone was studied, enhanced 1,3-allylic strain between the methyl and aldehyde could account for the regioselective outcome in this case.

Section 4: EXPERIMENTAL

Section 5.4.1. *General Procedures and Methods*

DFT calculations were performed using the Gaussian-16 software package. Structures were optimized at the wB97-XD/6-311++G(d,p) level of theory, using the PCM model with CH_2Cl_2 as solvent. Frequency calculations were performed on all structures and enthalpies and free energies were calculated using the harmonic approximation at standard state (1 M concentration). Free energies of activation have been adjusted and recorded for 0.04 M concentration to better reflect

the experimental conditions. All structures had zero negative frequencies, and the transition state had one negative frequency whose motions corresponded to the expected reaction coordinate.

Section 5.4.2. *Transition States*

Gaussian files are in Michael Group OneDrive/Berman/Thesis Calculation Files/Ene Special Cases. Table 5.1 conveys details of each transition states and the name of the corresponding Gaussian file.

Table 5.1. Filenames for Ene Transition States of Terpenes

Substrate	**C-H Activated**	**Filename (.log ending)**
Methyl Jasmonate	β to carbonyl	mjasabegc1142021mnbo1152021m
Methyl Jasmonate	ε to carbonyl	mjasaendcberny1142021mnbo1152021m
δ-Damascone	α to gem-dimethyl group	damasantiberny10202021mnbo10202021m
δ-Damascone	β to gem-dimethyl group	damasaqst210202021mnbo10202021m

REFERENCES FOR CHAPTER 5

[1] Hoekstra, W. J.; Fairlamb, I. J. S; Giroux, S.; Chen, Y. Selenium(IV) Oxide in Encyclopedia of Reagents for Organic Synthesis, Ed. Fuchs, P. L. 1−12 Wiley & Sons: 2017.

[2] Teh, W. P.; Obenschain, D. C.; Black, B. M.; Michael, F. E. *J. Am. Chem. Soc.* **2020,** *142,* 16716-16722.

[3] Zheng, T.; Berman, J. L.; *Michael*, F. E. *Manuscript Submitted.*

[4] Hoffmann, R. W. *Chem. Rev.* **1989,** *89,* 1841-1860.

[5] Johnson, F. *Chem. Rev.* **1968,** *68,* 375-413.